Authors' response to the Editor and both Referees
regarding
Review of : Lagrangian trajectory modelling for a person lost at sea. . ..
By Licer et al

The authors would first like to thank both the editor and both reviewers for taking the time to read and comment on the paper. We believe their comments led to a much improved and clearer revised version of the paper. Before we address their respective comments point-by-point below, we would like to briefly recapitulate major modifications to the paper content here:

- Independent verification of survivor's trajectory estimate is performed, using WERA HF radar back-propagation simulations from the beaching site. Both trajectories were found to be qualitatively consistent.
- A 10-month verification of the NEMO model was performed against HF radar data in the Gulf of Trieste. This allows us to put numbers on NEMO performance during the drift. Unfortunately this performance was below-average and this is now reflected in the paper where meridional and zonal model biases are stated.
- NEMO model description has been revised to indicate that HF radar data assimilation is not implemented at the time
- FlowTrack sections of the paper were left-out of the revised version since we agree with the review that OpenDrift-FlowTrack comparisons lacked added value to merit inclusion.
- Current-only and wind-only simulations were performed with "person with surf board" drifter type. Wind-only simulations are now included in the revised version of the paper and analyzed alongside full wind+current simulations.
- Quantitative estimation of performance of each simulation was added to the paper. We base these estimations on stranded and active particle distributions over distances from the beaching site. This allows us to quantify somewhat the performances of each simulation type even in the context of poor NEMO model performance. "Person with surf board" scenario yields also quantitatively the best results.
- Time lag of particle stranding at the beaching point was assessed from temporal dependence of particle distributions near the beaching site.

Our point-by-point responses are below. Reviewer suggestions are typed in **bold-face**, author responses (AR) are normally typed.

To me your recommendations in terms of effectiveness of the search strategy and for the survival of the windsurfer are not clear, neither in the abstract, nor in the conclusion. You simply comment that "search and rescue response should be as rapid as possible". This seems a rather trivial conclusion.

We thank the editor for this comment. We agree. This dictum has now been left out of the paper. Based also on other reviews, the whole paper was thoroughly rewritten to include less ambiguous and more quantitative analysis of Lagrangian model performance.

An example of questions that come to my mind is whether the search area (linearly increasing with time) could be effectively searched by a rescue vessel with reasonable chance to spot the windsurfer. Further, was the time needed for completing the simulation compatible with a timely rescue of the person lost at sea?

Thank you for this comment. We have now omitted the search-and-area formulations from the revised manuscript. We are not experts on search and rescue strategies, but we discussed this question with the Slovenian Civil Rescue service: first 15 hours after the incident, the rescue attempt was not possible due to severe conditions. They did in fact attempt marine and aircraft search and rescue action but it was not successful. Nevertheless, and given the limited dimension of the Gulf of Trieste, it was their opinion that timely rescue would have been possible – especially when guided by a reliable Lagrangian simulation.

It is not immediately clear from your text, but it seems that the whole model chain works in analysis mode, i.e. assimilating observations. Please, clarify this point in the text. If the results that you use are the results of an analysis, this would not be practically available during the actual search. How much does the result deteriorate if forecast fields are used?

We thank the editor for this comment. The text has been amended to show that NEMO does not at present have any data assimilation. Verification of the NEMO model versus ten months of hourly HF radar currents (not shown in this paper) yields a bias in zonal velocity between 0 and -2.5 cm/s and a bias between +2.5 and -2.5 cm/s for meridional velocity. NEMO model underestimations during the limited period of this case study were however even larger: spatially averaged (over the HF domain) and temporaly averaged (over the period of the drift) NEMO biases amounted to -6.3 cm/s for zonal velocity and a bias of -9.2 cm/s for meridional velocity. NEMO setup therefore exhibited below-average performance during the period of interest. This is now included in the paper. It also indicates that the model would benefit from HF radar data assimilation and we will be focusing on this in the future.

The subject of the paper is relevant, since it evaluates the performance of two Lagrangian models versus a real accident with a person lost at sea during an extreme meteorological event. The paper implementation though lacks in my opinion of several crucial elements. I therefore recommend re-submission, and ask the authors to address the points detailed in the following.

AR: We thank the reviewer sincerely for taking the time to read and comment on the paper!

1) In Section 1, the authors introduce the reconstructed trajectory of the survivor (Fig.1b), that they use to test the two proposed models. I find the trajectory and the associated uncertainty (500 m radius) quite arbitrary. Was the survivor in possession of a GPS, or at least of a watch (time information)? If so, this should be mentioned, and if not, how did he estimate time and position of the trajectory? In absence of solid information, I think that the evaluation should be based mostly on the only secure data point, which is the beaching point (in space and time) of the survivor, rather than trying to quantitatively match the specific positions evaluated along the trajectory.

AR: We thank the reviewer for this important question – we followed reviewer's instructions closely. No, the survivor was not in posession of a GPS or a watch. Therefore the reviewer is right to point out the arbitrary nature of his estimates. This reviewer's comment has - in conjunction with demands from the second reviewer – led to our independently verification of the survivor's drift trajectory. As described in a new passage in the paper this was done by interpolating in space and time the HF radar currents during the period of the drift, and to then use these measurements to compute Lagrangian *back*-propagation from the *beaching* location as the reviewer suggested. This simulation yields a trajectory which seems largely consistent with survivors estimate. We have explained trajectory verification in a separate section and plotted the results in Figure 4. We hope the reviewer will agree that this substantiation gives some credibility to the survivor's estimate and that we can use it as a qualitative orientation also during the drift, not only at the beaching point.

2) The description of the two Lagrangian models is inconsistent, the conceptual differences between the two are not clearly outlined, and a number of basic information that are then used later on in the paper, are not provided. Specifically, why is the particle equation written for Flow Track (Section 4.2, eq 1) and not for OpenDrift (Section 4.1)? If the basic equation is the same, it should be introduced in Section 4.1 and the differences in parameterizations and considered processes should be discussed up front, for instance in terms of wind drag and lift, Stokes, turbulence etc..
Also the model implementation should be better discussed. How many particles are typically launched in each model? (this is mentioned for Flow Track but not for OpenDrift) How are the results diagnosed? In Section 5, it is mentioned that for OpenDrift a Rescue Area (RA) is computed as a polygon based on particle

location, while in Section 5 and 6, it is mentioned that a RA cannot be computed for Flow Track. . . I do not understand why is it so, and I think it should be better explained. Also, all these aspects should be presented up front in Section 4, rather than at the end of the paper.

AR: We thank the reviewer for this comment. We agree that the two Lagrangian models are different in many respects and this is often an issue when comparing different model performances. After both reviewers pointed out this comparison as a weakness of the paper, we decided to leave FlowTrack section out and instead deepen the OpenDrift part.

Now there is only one Lagrangian model in the paper (OpenDrift), but it is presented in more depth and used in more ways. It is used for back-propagation trajectory verification on HF currents and subsequently for forward-propagation with modelled currents. We hope this lessens the confusion and clarifies the paper.

However, to answer the reviewer's question about RA in FlowTrack: the RA can of course be computed also for FlowTrack which, as reviewer mentions, should indeed have been pointed out in the first version of the paper. However the particles in Flowtrack simulations form a very thin sickle(y) geographic shape so the actual RA is misleadingly small and therefore not very telling. This question however has now been put aside since FlowTrack was omitted in the new version of the paper.

3) The discussion of model evaluation in Section 5 is in my opinion very unclear. The paragraphs at pg12 and 13 for PIW and PPV are simply repeated with the RA values changed. . .What are the grey shading areas shown in Fig. 8-10 and how are they computed? I do not see a clear difference in the three cases. The authors seem to favor the results of OpenDrift PPV because the RA is more reduced (even though it still covers the whole Gulf?), but the RAs are not shown in the figures. In general, as mentioned in point 1) I think that the quantitative assessment should be based mostly on the beaching point. What is the distribution of beached particles time and space for the 3 configurations?

AR: We thank the reviewer for the suggestion. We have followed it and we now include the calculation of the distribution of stranded and active (still in the water column) particles and plotted its histogram over distances from the beaching location at beaching time for both drifter types. These plots are now depicted in Figure 10 in the paper. The following analysis was added to the paper:

"Top right panel in Figure 10 indicates that the distribution maximum of "person with surf board" drifters is positioned about 12 km closer to the beaching point than the distribution maximum of "person in water" drifters. The fact however that the distribution maximum of "person with surf board" drifters is also positioned about 12 km from the beaching point indicates that there is a lag in the movement of these drifters. As mentioned above, this is very likely due to the NEMO model surface current estimation during the event. These conclusions are also consistent with spatial particle distributions in Figures 8 and 9: at beaching time, "person in water" particles are dispersed over a much wider area than those of "person with surf board" type. Top right panel of Figure 10 reflects that.

However, and regardless of this lag, when focusing on the accumulation of stranded particles (bottom left panel of Figure 10), we may reach a conclusion that at beaching time about twice as many "person with surf board" drifters stranded within 5 km of the beaching point than those of "person in water" type. The same holds for particles stranding within 10 km radius. Within 20 km radius this ratio triples. All these results quantitatively substantiate earlier qualitative claims of better performance of the "person with surf board" drifter type for this case study."

Included in the mentioned section are also wind-only simulations results, treated in the same fashion as indicated in the passage above.

We also performed new simulation runs beyond the beaching time to estimate time-lag of particle arrivals. For all drifter types, stranded particle distributions begin to saturate roughly six hours after the beaching time. This result has now been included as the B panel in Figure 10.

4) The conclusions (Section 6) are in my opinion not satisfactory. The authors mention that OpenDrift is more suitable for Search and Rescue applications because it is more operational, i.e. it has a classification for object parametrizations, and it provides Ras. But these points were known from the beginning, given the model characteristics! What is the added value of the comparison?
I think the authors should discuss in an objective way the results, and indicate strength and weakness of each model with respect to the actual performance. Of course,is also important to point out the shortcoming of Flow Track in terms of operational performance, but indeed that was a given and we did not need this exercise to reach this conclusion. . .

AR: We agree that there was too little added value to the original model comparison and that it does not warrant publication. Flowtrack is now out of the paper.

5) Finally, I would like to make a general comment. From the patterns of currents and wind (Fig.5,7), it looks like the trajectory of the survivor was likely to be strongly influenced by the ocean currents (that facilitate the entrance inside the Gulf,) while the trajectories of both models tend to overestimate the wind influence (that moves them more to the north-west).
Indeed Fig.6 shows that the wind input in the Lagrangian models is approximately double with respect to the currents (please clarify the dimensions of the variables that Figure: are they velocities or are they model inputs somehow normalized?).
On the other hand Fig.5 shows that the NEMO current amplitude is underestimated with respect to the HF radar. So, it is possible that improving NEMO results would greatly improve the trajectories of the Lagrangian models. Alternatively, could the HF radar results be used as inputs in the Lagrangian models? I understand that there is a permanent gap in the middle of the Gulf, likely due to the GDOP, but probably gap filling techniques can be used in it in to ensure a more extended coverage. The authors should explore these aspects.

AR: We agree with this comment and thank the reviewer for it. This comment, in conjunction with the first comment, led to gap-filling of the HF radar data and to the performing of back propagation from the beaching location.

Since back-propagation from the beaching location using HF radar currents is consistent with survivor's trajectory at the beginning and at the end, we believe the reviewer is right: improving NEMO results would lead to an improvement of Lagrangian tracking.

As we now point out in the paper, we performed a 10 month verification on HF radar data with NEMO and it seems the model performance during the Scirocco was particularly weak since the biases in (u,v) currents are otherwise much lower. Verification of the NEMO model versus ten months of hourly HF radar currents (not shown in this paper) yields a bias in zonal velocity between 0 and -2.5 cm/s and a bias between +2.5 and -2.5 cm/s for meridional velocity. NEMO model underestimations during the limited period of this case study were however even larger: spatially averaged (over the HF domain) and temporaly averaged (over the period of the drift) NEMO biases amounted to -6.3 cm/s for zonal velocity and a bias of -9.2 cm/s for meridional velocity. NEMO setup therefore exhibited below-average performance during the period of interest. This issue with model performance during storm conditions was explicitly pointed out in the paper and will have to further addressed in a separate investigation.

As far as Fig 6 is concerned, thanks for pointing this out. Plotted quantities are drifts, and therefore Eulerian velocities (in case of currents) or OpenDrift downwind slopes x u10 (in case of winds). Units are m/s. No other normalization is used. All this is now explicitly stated in the Figure caption.

In this work the potential trajectory followed by a windsurfer lost at sea in the surroundings of the Gulf of Trieste during a storm that took place in October 2018 is simulated through a Lagrangian approach.
To this end, high resolution oceanic and atmospheric models are used as input for two Lagrangian tools: OpenDrift and FlowTrack. Despite using the same numerical integration scheme (Runge-Kutta 2nd order) they present some differences. Likely the most important is that Open Drift offers pre-calibrated coefficients for downwind and crosswind components more suitable to simulate the drift of a person at sea, specially if the wind drift is dominant. As a result, the final distribution of particles simulated by OpenDrift match better the (tentative) inferred trajectory reconstructed by the authors from an interview with the windsurfer.

My impression is that this paper is based on a compelling idea and that results can be potentially useful at regional and operational level. English is good and one key strength is that model data (especially ocean currents) have very high resolution. However, I feel that this version of the manuscript needs some reorganization, a more accurate description of methods, a more elaborated assessment of the different con tributions of wind/ocean currents/(waves?) terms to the simulated trajectories, and an improved treatment of uncertainties and search and rescue areas, before being considered suitable for publication.

AR: We thank the reviewer sincerely for taking the time to comment on the paper!

In the below lines I elaborate further my above overall impression.

Major Comments
A- It is rather weird (and a bit confusing) to describe wave data from ECWAM model when it is not used later in the Lagrangian simulations. Indeed I think it is more logic to start in Section 2 with the quite general equations of Lagrangian particle tracking (current Section 4), and later describe in Section 3 observations and model data. In this way the fact that you neglect the Stokes drift is clearly stated and there is no need to include a description of the wave model in Section 3. Then in Section 4 you could show the results on the validation of model data with observations, and so on.

AR: We thank the reviewer for the comment. We agree that the approach was confusing. Before we clarify changes to the revised paper any further, we would like to say the following in our defense: it is true that ECWAM was not used in the final simulations with FlowTrack. But we did need ECWAM to compute the surface gravity wave wavelengths and to justify that we may indeed neglect Stokes drift. So we needed ECWAM to decide if we need it or not. This is why it was eventually presented. Since FlowTrack is out of the revised manuscript, ECWAM is also out of the paper. With OpenDrift this was not an issue since its parametrizations already include wave effects and OpenDrift consequently does not require the wave model at all. We also hope the existing section order is now working better.

Additionally, OpenDrift is now presented in more depth and additional simulations were made. We will address these changes point by point below.

B- You say that you do not consider the Stokes drift for your simulation because wavelengths are significantly larger than the size of a person/windsurf table. However, as far as I understand in the case of microplastics, wavelengths are proportionally even larger but the Stokes drift has an important role on their distribution (e.g. van den Bremer and Breivik; Onink et al., 2019). Am I wrong? I think that it is likely simpler to say that the Stokes drift is generally a second (or third) order term in the Adriatic Sea in terms of magnitude (e.g. see Fig. 1d within Onink et al., 2019) . Indeed it would be a good exercise to verify this point with an in-situ wave buoy or with your wave model data.

AR: As pointed out above, we now leave sections of FlowTrack, and consequently ECWAM, out of the revised paper. However, we will try to respond to the reviewer's

question. Stokes drift is computed as a temporal mean of Lagrangian water particle velocity over its unclosed orbit in a surface gravity wave. It is in principle computed for the water particle moving passively with the wave field, not for material objects in the water. Although this is not a specialty of any of the authors, we would expect that the microplastics can safely be said to move directly with the fluid in the wave field. On the other hand, as far as we understand, there seems to be a difficulty to claim the same for larger material objects. Their orbits in the wave field do not generally follow closely the fluid motion due to a gravity wave. Therefore the temporal mean of the *object's* Lagrangian velocity over one cycle of its orbit, i.e. its "Stokes" drift, may differ substantially from the temporal mean of the surrounding *fluid's* Lagrangian velocity, i.e. water's Stokes drift. The argument was made in the references cited in the original version of the paper (Hackett et al. 2006, Breivik and Allen 2008) that we can only assume that object's orbit coincides to any significant degree with surrounding fluid particles orbits if the length of the material object is close to the surface gravity wave wavelength. In this case, Stokes drift calculation for fluid is a good estimate for the temporal mean of the object's unclosed orbits in the wave field. In other cases the orbits differ too much to make this assumption. This is how we understand the issue.

C- It is not explained which expression you use to simulate turbulent effects (random numbers) at each time step. Is it based on a uniform or a normal distribution? Is it different for each direction? Is the maximum number of 0.02 m/s based on observations or a model assessment? Indeed in coastal regions where strong gradients in ocean currents exist the magnitude of diffusivity can change significantly between relatively close grid cells depending on the ocean features. Please clarify this point.

AR: As noted above, FlowTrack was removed from the paper. Turbulent component was however computed from a normal distribution around this value (for each direction) which was inherited from an older Lagrangian code (unpublished), which based it from empirical vertical velocity shear data from some specific nice-weather situations (unpublished). We are aware that a constant turbulent diffusion is unacceptable for velocity fields with significant shear and we are improving FlowTrack to be able to ingest NEMO horizontal eddy viscosities, obtained via Smagorinsky or other schemes which take into account local velocity shear.

D- With respect to the validation of the model data with observations, why do not show a comparison between the ADCP data (Figure 6, violet arrows) and the closest grid cell ocean model velocity? This would help to provide some numbers on the discussed underestimation of modeled currents. Also, do you have any reference in which HF radar velocities have been validated? Add it (them) to Section 2.2.

AR: We thank the reviewer for the suggestion. We have followed it to perform a 10-month verification of the NEMO model against surface current HF radar data. We hope the reviewer will agree that this is a more extensive way to verify NEMO than a single-point ADCP comparison. We do not show plots of the results but we do state numerical values of the errors in the updated revision of the paper: they unfortunately indicate below-average model performance during the period of the drift and this is clearly pointed out in the paper.

The following passage was added to the paper: "Verification of the NEMO model versus ten months of hourly HF radar currents (not shown in detail in this paper) yields a bias in zonal velocity between 0 and -2.5 cm/s and a bias between +2.5 and -2.5 cm/s for meridional velocity. NEMO model underestimations during the limited period of this case study were however even larger: spatially averaged (over the HF domain) and temporaly averaged (over the period of the drift) NEMO biases amounted to -6.3 cm/s for zonal velocity and a bias of -9.2 cm/s for meridional velocity. NEMO setup therefore exhibited below-average performance during the period of interest. This will have to be further addressed as a separate issue and needs to be kept in mind when interpreting results below.
"

E- Other unclear points are:
- How do you estimate the light red circles in Fig. 8-10?
AR: We thank the reviewer for this question. These were initial estimates by the survivor. We now expand on our reply to the other reviewer in this regard. The survivor was not in posession of a GPS or a watch. Therefore both reviewers have justification to point out the arbitrary nature of his estimates. They are indeed arbitrary but we nevertheless took them as a rough estimate – this reviewer's comment has - in conjunction with demands from the second reviewer – led to our independently verification of the survivor's drift trajectory. This was done by interpolating in space and time the HF radar currents during the period of the drift, and to then use these measurements to compute Lagrangian *back*-propagation from the *beaching* location. This simulation yields a trajectory which seems largely consistent with survivors estimate. We have explained trajectory verification in a separate section and plotted the results in Figure 4. We hope the reviewer will agree that this substantiation gives some credibility to the survivor's estimate and that we can use it as a valuable qualitative orientation also during the drift, not only at the beaching point.

- Why particles are initially deployed in a rectangular shape?
AR: The square shape was simply one of the ways particles are seeded in FlowTrack. We comment a bit more below.

- You deploy initially 480 particles, one for each value of Lp(theta), however in this way the uncertainty introduced by their different initial location is not assessed. What is the impact of the uncertainty in the initial position on the final search and rescue area for each Lp(theta)? Is it significant?
AR: We thank the reviewer for this question. Yes, this is a good point. We haven't tested this sensitivity specifically but it is perhaps worth noting that the model resolution is 1 km and the deployment square size is 1 km. Therefore the dimension of the deployment shape is equal to the model grid size. Therefore we would expect that in this case the uncertainty in the initial position would not have, in itself, significant impact on the SAR areas since the model velocities change very little over the dimension of the release shape. However, note again that FlowTrack passages were removed from the paper.

F – I find that would be interesting to show also the distribution of simulated particles with only wind drift/only ocean currents, and to estimate how large is the dispersion of particles (final area of search and rescue) for both cases. It would show graphically how predominant is the wind drift in the advection of particles and the lag with only ocean current.

AR: We thank the reviewer for the suggestion: we have performed both (wind-only / current only) simulations for "person with surf board" drifter type as the reviewer suggested. We include the results below. Wind-only particle simulations were also included in the revised Figure 9 and in Figure 10 and we comment upon them in the text as well. Given that the situation was wind dominated, as is clear from "wind+current" and "wind-only" simulations, we did not include "current only" simulations in the paper.
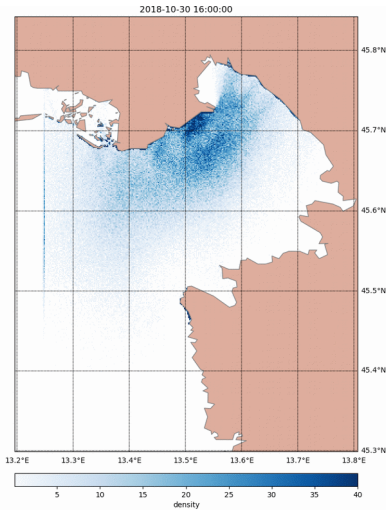
Wind-only particle distribution after last time step:
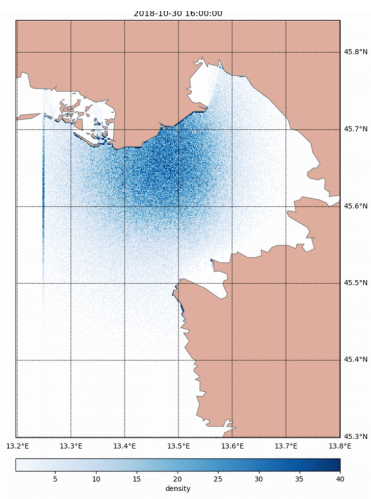
Current-only particle distribution after last time step:
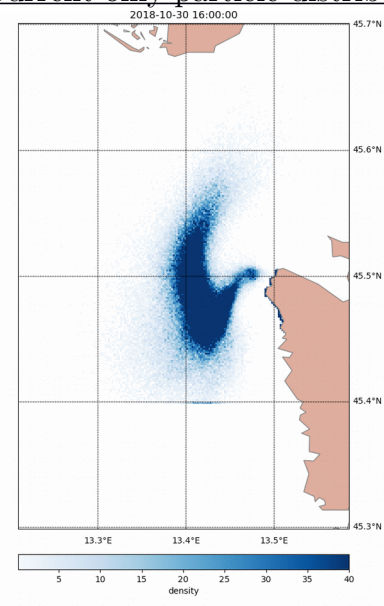
<u>Wind+current distribution</u> at the last timestep:

These figures indicate that winds are the dominant factor in this drift, but the currents play their role in elongating the spread along the coastal current "jet" direction (seen in left panel of Figure 6) thus moving it closer towards the beaching site.

G- My major criticism to this work is the approach you follow to show your results. Considering that it is aimed to be useful for search and rescue (SAR) tasks and, therefore, time is critical, I think that to show trajectories is far less useful than to show areas (or contours) of accumulated probability constructed with suitable mathematical functions. In terms of accumulated probability the areas for search and rescue tasks can be more easily prioritized. Your estimated areas after just few hours of simulation look pretty large to be useful for search and rescue tasks. Additionally, the probabilistic approach naturally includes the fact that there are uncertainties everywhere. Even more, probability contours can have a bimodal distribution, while your polygon seems to include all particles inside irrespective of the spatial holes among them. For example, this approach can be found in Abascal et al., (2010). You need to convince me that for SAR tasks your current approach is reasonable enough, otherwise I suggest to redo your Fig. 8-10 with a probabilistic perspective (showing e.g. contours of 50%/70%/90% of accumulated probability estimated from the distribution of your particles), which is relatively easy to implement. In the latter case I suggest to remove the word "trajectory" from the title.

AR: We thank the reviewer for the suggestion: we have rerun and replotted all simulations with OpenDrift to show numerical particle densities [number of particles / m2] which are a proxy for the probability of finding the particle on a given location at a given time (i.e. number of particles in a cell / number of released particles). Particle spread of modeled drifter types is in our case however very large and leads to very small probabilities on the scale of 1e-4 to 1e-5. We decided such numbers are not very telling and that particle density maps perhaps seem more intuitive to the reader. This density approach has been commonly used by the authors of OpenDrift themselves (Roehrs et al, 2018; Dugstad et al, 2019). We hope this satisfies the reviewer. We have followed reviewer suggestion and removed the word "trajectory" from the title.

Other Comments
Title. Change "for" by "of".
AR: Done.

Ln 2. Suggest to change "He was drifting" by "He drifted".
AR: Done.

Ln 6. We "modeled".
AR: This is now out of the text.

Ln 52. Unclear how you estimate the +/- 500 m of error.
AR: As noted, this is survivor's subjective estimate. We now state this in the paper explicitly and we add independent verification of survivor's trajectory using back-propagation on HF radar currents.

Ln 65. "By the time he is entering" . . .
AR: Done.

Ln. 218. Remove point after "day"
AR: Done.

Ln. 218. "all directions..."
AR: Done.

Ln. 224. "generates a westward initial current".
AR: Changed to "generates a westward inertial current"

Lagrangian ~~Trajectory~~ Modelling ~~for~~ of a Person lost at Sea during Adriatic Scirocco Storm of 29 October 2018

Matjaž Ličer[1], Solène Estival[2], Catalina Reyes-Suarez[3], Davide Deponte[3], and Anja Fettich[4]

[1]National Institute of Biology, Piran, Slovenia
[2]École Nationale Supérieure de Techniques Avancées, Paris, France
[3]Istituto Nazionale di Oceanografia e Geofisica Sperimentale, Sgonico, Italy
[4]Slovenian Environment Agency, Ljubljana, Slovenia

Correspondence: Matjaž Ličer (matjaz.licer@nib.si)

Abstract. On 29 October 2018 a windsurfer's mast broke about 1 km offshore from Istria during a severe Scirocco storm in the Northern Adriatic Sea. He ~~was drifting~~ drifted in severe marine conditions until he eventually beached alive and well in Sistiana (Italy) 24 hours later. We conducted an interview with the survivor to reconstruct his trajectory and to gain insight into his swimming and paddling strategy. Part of survivor's trajectory was verified using high-frequency radar surface current observations as inputs for Lagrangian temporal back-propagation from the beaching site. Back-propagation simulations were found to be largely consistent with survivor's reconstruction. We then attempted a Lagrangian forward-propagation simulation of his trajectory ~~in two ways. Firstly~~ by performing a leeway simulation using the OpenDrift tracking code using two object types: ~~Person-in-Water-1 and Person-powered-vessel-2. Secondly, we model the trajectory using our own Lagrangian tracking code FlowTrack~~i) person in water in unknown state and ii) person with surf board. In both cases a high-resolution (1 km) setup of NEMO v3.6 circulation model was employed for the surface current component and a 4.4 km operational setup of the ALADIN atmospheric model was used for wind forcing. ~~OpenDrift yields best results using Person-powered-vessel-2~~ Best performance is obtained using "person with surfboard" object type, ~~indicating a relatively broad search and rescue area which covers 45 km² after six hours and rises to 380 km² after 24 hours. The simulated most probable SAR area envelops the reconstructed drift trajectory and is also temporaly consistent with the reconstruction. FlowTrack yields a search and rescue area with a comparable lateral extent but with much less downwind spread. While both Lagrangian models were able to envelop the reconstructed drift trajectory during this validation, we recommend using OpenDrift for similar search-and-rescue missions in the future due to its flexibility and drifting object dependent calibration on empirical data~~giving the highest percentage of particles stranded within 5 km of the beaching site. Accumulation of particles stranded within 5 km of the beaching site saturates 6 hours after the actual beaching time for all drifter types. This time-lag most likely occurs due to NEMO underestimation of surface currents during the period of the drift. A control run of wind-only forcing shows the poorest perfomance of all simulations. This indicates the importance of topographically constrained ocean currents in semi-enclosed basins even in seemingly wind-dominated situations.

1 Introduction

Lagrangian particle tracking of objects lost at sea is an important branch of ocean forecasting. Maritime search and rescue (SAR) or other types of civil service responses depend on timely and reliable estimates of the most probable areas which contain the drifting object. These estimates generally require prior computation of ocean currents, waves and winds in the area, which are most often provided by numerical circulation, wave and atmosphere models.

The wind force contribution to the objects drift is termed its leeway and has both downwind (drag) and crosswind (lift) component (Breivik and Allen, 2008). The object's drift therefore generally deviates from the wind direction by some divergence angle L_α (Allen and Plourde, 1999), related to the downwind and crosswind components. Specific values of the object's downwind and crosswind drift are determined by the balance of the wind (lift and drag) force on the overwater part of the object and the hydrodynamic (lift and drag) force on the subsurface part of the object - object's drifting properties therefore depend significantly on its shape. Empirical observations have consequently been the most straightforward method of determining the drifting parameters for various drifting object types, including human bodies (Allen and Plourde, 1999; Hackett et al., 2006). Reports on marine drifts involving survivors are not ubiquitous, which makes reviews like (Allen and Plourde, 1999) all the more valuable for any attempt to accurately model the drift of a person or any other object.

In this paper we focus on an incident which occured on 29 October 2018 in the Northern Adriatic Sea and led to a 24 hour drift of a person in gale wind conditions (level 8 on Beaufort scale). For an extensive analysis of the atmospheric and marine conditions during the 29 October 2018 storm the reader is referred to Cavaleri et al. (2019). These conditions are related to the fact that the Adriatic sea is a northwest-southeast oriented elongated basin of the Northern Central Mediterranean, exchanging properties with the eastern Mediterranean basin through the Otranto strait (19° E, 40° N in Figure 1 a)). It is 800 km long and 200 km wide and surrounded from all sides by mountain ridges - the Alps in the north, the Apennines in the west and Dinaric Alps in the east. These ridges exhibit significant influence on the basin circulation through topographic control of the air flow, most notably during episodes of the northeasterly Bora wind and southeasterly Scirocco. The northern part of the Adriatic is a shallow shelf with depths under 60m. Its northernmost part, extending into the Gulf of Trieste, is the shallowest, with depths around 20 to ~~30m~~ 30 m (see Figure 1 b)).

~~a) Adriatic basin bathymetry. Abbreviations are as follows: VE - Venice, IP - Istrian Peninsula, N Adr Shelf - Northern Adriatic Shelf, OT - Otranto Strait. Direction of Scirocco is marked with white arrow. b) The Gulf of Trieste and piecewise trajectory of the drift as estimated by the survivor. Location estimates are junctions of the piecewise straight line. Circles denote location uncertainty estimates at specific times. The cyan 'x' sign north of Piran denotes the location of the Vida coastal buoy. Background layer is Sentinel-2 L1C True Color image of the Gulf of Trieste from the day after the beaching, 31 Oct 2018 (obtained from Copernicus Open Access Hub: https://scihub.copernicus.eu). Turbid Soča/Isonzo river plume is clearly visible along the northern shore of the Gulf.~~

In the afternoon of 29 Oct 2018, the Scirocco speeds along the west coast of northern Istria were in the range 15-25 ~~m s~~ m s^{-1} and significant wave heights amounted to 3-5 ~~m~~ m (Cavaleri et al., 2019), while maximum wave heights in the southern part of the Gulf of Trieste at coastal buoy Vida (see Section 2.1 for details and Figure 1 b) for location) were observed to be

over 2.5 ~~m~~ m (not shown). The town of Umag in northern Istria is a popular windsurfing spot during Scirocco conditions: on 29 Oct 2018 many people were windsurfing there when the accident occured at estimated 16 UTC. The windsurfer's mast broke roughly 1 km offshore northwest of Umag (see Figure 1 b) for location) initiating the drift. The conditions were too severe for immediate marine rescue either by his colleagues or by authorities. A joint Italian, Croatian and Slovenian SAR mission was initiated next morning (30 Oct 2018) but it was unsuccesful - the surfer beached on his own 24 hours later close to Sistiana north of Trieste (see Figure 1 b)). The windsurfer's harness was however recovered in the central part of the Gulf of Trieste at around 15 UTC on 30 Oct.

The survivor kindly responded to our interview request. He is an experienced windsurfer and has been windsurfing along the coasts of Gulf of Trieste for the past 30 years. We state that explicitly to convey the fact that he knows this coastline very well. We now briefly recapitulate his personal statements about the drift. He was conscious and focused the entire time. The visibility was not bad and he could see the coastline of the Gulf of Trieste in its entirety, which helped him make mental notes of his location. He was highly alert to his location throughout the drift but did not have a watch or a GPS. We have therefore attempted to independently validate his trajectory estimate, as will be explained bellow in Section 4.1.

His mast broke on 29 Oct 2019 16 UTC at 13.625° E, 45.558° N with an estimated ± 500 ~~m~~ m error in each direction, see Figure 1 b) for location.

Immediately after the accident, he drifts alongshore north of Umag and he actively paddles towards the coast, hoping to reach the Cape of Savudrija. The wind direction at his location is however slightly offshore and sometime between 19.30 and 20.30 UTC he realizes he will not be able to reach Savudrija. ~~He releases his windsurfing harness in the water.~~ After 20 UTC the Scirocco strengthens. He is now located northwest of Savudrija, drifting north-northwest toward Grado. Swimming is not possible due to airspray and sea conditions, but he keeps shaking his arms and legs interchangeably to keep warm. At some point between 20 UTC and 23 UTC he can see the town of Izola (Slovenia) and the town of Grado (Italy) at right angles. It is around 23 UTC that his drift turns north-east. After 23 UTC, he is located approximately on the Piran-Grado line. Sea conditions get very severe, he is laying on the windsurf board, mostly facing southwest, away from the mean drift direction, drifting backwards, clutching the footstraps on the surfboard. He estimates that every 50th wave breaks over him and pulls the surfboard from under him. When this happens he needs to wait to reach the crest of the wave to visually re-locate the board and catch it. In the morning, on 30 Oct 2019 07 UTC, he is located 2 - 4 km south-southwest of the Soča/Isonzo river mouth. By 9-10 UTC he is located roughly 1-2 km south-southeast of the river mouth and the water gets significantly colder as he likely enters the Soča/Isonzo river plume (visible in Figure 1 b)). By the time ~~of his~~ he is entering the plume, the Soča/Isonzo runoff is at a several-month maximum, as depicted in Figure 2. From 11 UTC on he is paddling actively toward northeast to overcome the riverine westward coastal current until he reaches the beach near Sistiana at 16 UTC.

The drifting trajectory, reconstructed from above, is shown in the b) panel in Figure 1. Due to the nature of the testimony and lack of measuring equipment, survivor's trajectory is burdened with error. Survivor estimated the errors in his spatiotemporal location to best of his ability: these estimates are presented as semi-transparent circles around each marked location in Figure 1 and other Figures. We have however attempted to verify the final part of his trajectory by using high-frequency radar surface current measurements to perform Lagrangian back-propagation of particles from his beaching location back into
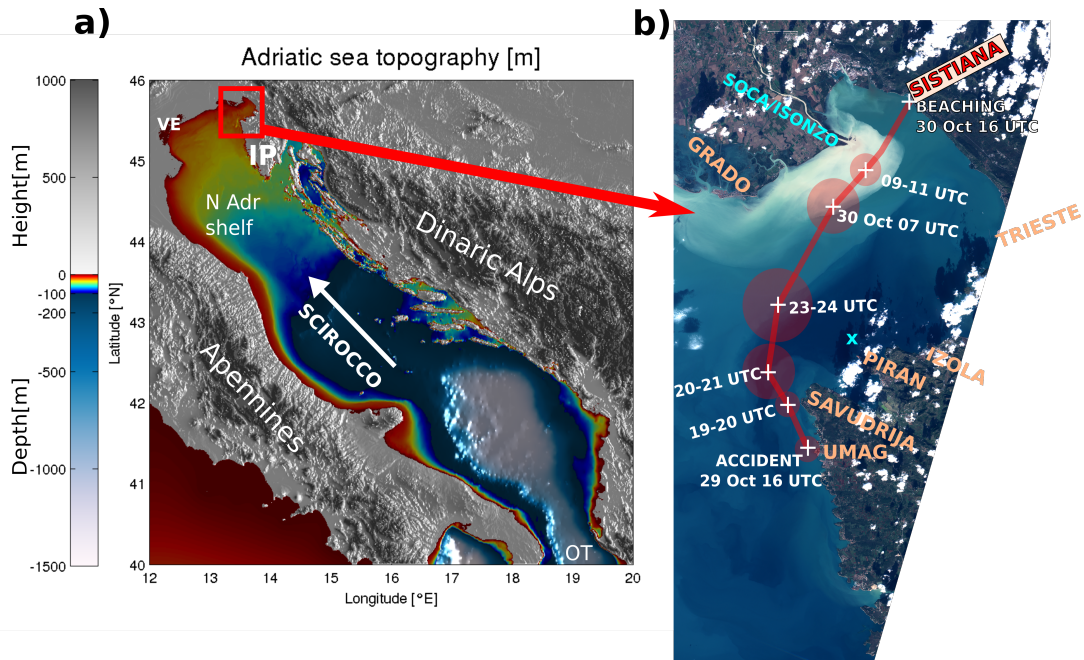
Figure 1. a) Adriatic basin bathymetry. Abbreviations are as follows: VE - Venice, IP - Istrian Peninsula, N Adr Shelf - Northern Adriatic Shelf, OT - Otranto Strait. Direction of Scirocco is marked with white arrow. b) The Gulf of Trieste and piecewise trajectory of the drift as estimated by the survivor. Location estimates are junctions of the piecewise straight line. Circles denote location uncertainty estimates at specific times. The cyan 'x' sign north of Piran denotes the location of the Vida coastal buoy. Background layer is Sentinel-2 L1C True Color image of the Gulf of Trieste from the day after the beaching, 31 Oct 2018 (obtained from Copernicus Open Access Hub: https://scihub.copernicus.eu). Turbid Soča/Isonzo river plume is clearly visible along the northern shore of the Gulf.

92 the Gulf. As will be shown later, these results are consistent with survivors trajectory estimate. While not allowing for any
93 meaningful quantitative verification of the Lagrangian codes in this paper, we believe that the trajectory is a qualitatively
94 suitable benchmark for our simulations.

95 In the present paper, we present two attempts to simulate this trajectory using ~~two different particle tracking models,~~
96 ~~OpenDriftand FlowTrack~~ state-of-the-art particle tracking model OpenDrift. Available observations and general marine con-
97 ditions during the drift are presented in Section 2; numerical models used for particle tracking modelling chain are described
98 in Section 3. Lagrangian ~~models are~~ model OpenDrift and its setup is presented in Section 3.1. Simulation results are depicted
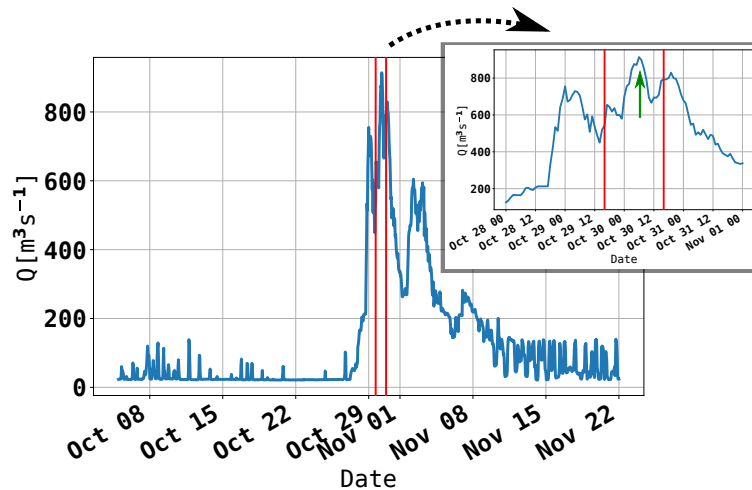99 and discussed in Section 4, followed by concluding remarks in Section 5.

Figure 2. Soča/Isonzo runoff during October and November 2018, as measured at an upstream river gauge (operated by ARSO) at Solkan, Slovenia. Vertical red lines indicate the timewindow of the drift. Green arrow in the inset marks approximate time of windsurfer's entering the river plume.

2 Observations

2.1 Coastal buoy Vida

The oceanographic buoy Vida is a coastal observation platform, operated by the Marine Biology Station at the National Institute of Biology (NIB). It is located in the southern part of the Gulf of Trieste at (13.55505 E, 45.5488 N), see b) panel of Figure 1 (marked with a cyan cross). Data from the buoy are multifaceted (air temperature, air humidity, currents, waves, sea temperature, salinity, dissolved oxygen, chlorophyll concentration, etc.) and are publicly available (http://www.nib.si/mbp/en/buoy/) in near real time. Ocean currents are acquired by a Nortek AWAC acoustic Doppler current profiler, mounted on the sea bottom at a depth of 22.5 m, to monitor vertical current profiles (at 1 ~~m~~ mintervals along the water column). The top most cell of the ADCP measurement corresponds to a depth around 0.5 m. Further information on the buoy can be found in Malačič (2019).

2.2 High Frequncy Radar System

The HF systems deployed in the Gulf of Trieste consist of two WERA stations (Gurgel et al., 1999) manufactured by Helzel MessTechnik in Germany, one at the OGS facility in Aurisina (Italy) and the second, operated by NIB, in the urban area of Piran (Slovenia). The systems provide sea surface current maps since January 2015. They rely on the scattering of a short-duration (9 minutes) and low-power (below 20 Watts) harmless radio wave pulses from waves at the ocean surface satisfying the Bragg-resonance scattering condition for coherent return. The two systems operate at a carrier frequency of 25.5 MHz as regulated by the International Telecommunication Union, covering the Gulf of Trieste at 1 ~~km~~ km range resolution and 1° angular resolution every 30 minutes. After aquisition, data are processed and radial components of the surface current field

5

117 are obtained, which in turn are combined into a 1.5 ~~km~~ km horizontal resolution 22×20 regular grid (see Figure ~~6~~ 3 for

118 coverage during the event and both station locations). Combined data are stored in databases and can be visualized in near real

119 time at http://www.nib.si/mbp/en/oceanographic-data-and-measurements/other-oceanographic-data/hf-radar-2. WERA system

120 external antenna field calibration was performed in 2016 and WERA system intrinsic estimates of zonal and meridional current

121 errors amount to 1-3 cm s^{-1} (roughly 3 - 10% of observed current speed) during the period of the drift. Data availability during

122 the 24 hours of the drift was between 50 and 70 percent, as depicted in Figure 3. The two WERA HF systems are operated and

123 maintained in collaboration between researchers, engineers and technicians from OGS and NIB.

3 Models

3.1 Ocean ~~, Wave~~ and Atmospheric Models

3.1.1 NEMO Circulation Model

127 We are using a high horizontal resolution (1°/111 or roughly 1000 m) setup of NEMO v3.6 (Madec, 2008) over the Adriatic

128 basin on a regular 999×777 longitude-latitude grid and 33 vertical z^*-levels with partial step. Model domain spans $12° - 21°$ E

129 and $39° - 46°$ N, see Figure 3. Maximum vertical discretization stretch is located at 15th level to allow for appropriate vertical

130 resolution near the surface. In all regions shallower than 2 ~~mm~~ m, a minimum 2 ~~m~~ m depth is enforced. Vertical level depths in me-

131 ters are 0.50, 1.51, 2.55, 3.64, 4.83, 6.20, 7.94, 10.38, 14.18, 20.56, 31.68, 51.23, 84.58, 137.94, 215.83, 318.24, 440.67, 576.90,

132 721.55, 870.95, 1022.92, 1176.25, 1330.29, 1484.69,1639.28, 1793.97, 1948.71, 2103.47, 2258.25, 2413.03, 2567.81, 2722.60,

133 2877.39. Explicit time-splitting is enforced and barotropic timestep is automatically adjusted to meet Courant-Friedrichs-Lewy

134 stability criterion. Baroclinic timestep was set to 120 s. The model is ~~hotstarted daily~~ running daily at Slovenian Environment

135 Agency (ARSO). It is initialized from previous operational run. Hourly lateral boundary conditions in the Ionian Sea are

136 taken from the Copernicus CMEMS MFS model. Turbulent heat and momentum fluxes across the ocean surface are computed

137 with CORE bulk flux formulation (Large and Yeager, 2004) using ALADIN SI atmospheric fields (surface wind, cloud cover,

138 mean sea level pressure, 2m temperature, relative humidity and precipitation). Rivers are implemented as freshwater release

139 over the entire water column at the discharge location, with runoff values as described in Ličer et al. (2016). Tides are in-

140 cluded as lateral boundary conditions for open boundary elevations and barotropic velocities for K1, P1, O1, Q1, M2, K2, N2

141 and S2 constituents. Constituents at the open boundary are obtained using OTIS tidal inversion code (Egbert and Erofeeva,

142 2002), based on TPXO8 atlas. The model employs Flather boundary condition for barotropic dynamics and Flow Relaxation

143 Scheme (Engedahl, 1995) for baroclinic dynamics and tracers at the open boundary. Lateral momentum boundary condition

144 at the coast is free-slip. Bottom friction is nonlinear with a logarithmic boundary layer. Lateral diffusion schemes for tracers

145 and momentum are both bilaplacian over geopotential surfaces. Vertical diffusion is computed using Generic Length Scale

146 (GLS) turbulence scheme. Craig and Banner formulation (Craig and Banner, 1994) of surface mixing due to wave breaking is

147 switched on. Present NEMO setup does not have data assimilation and all the simulations in this paper consequently lack any
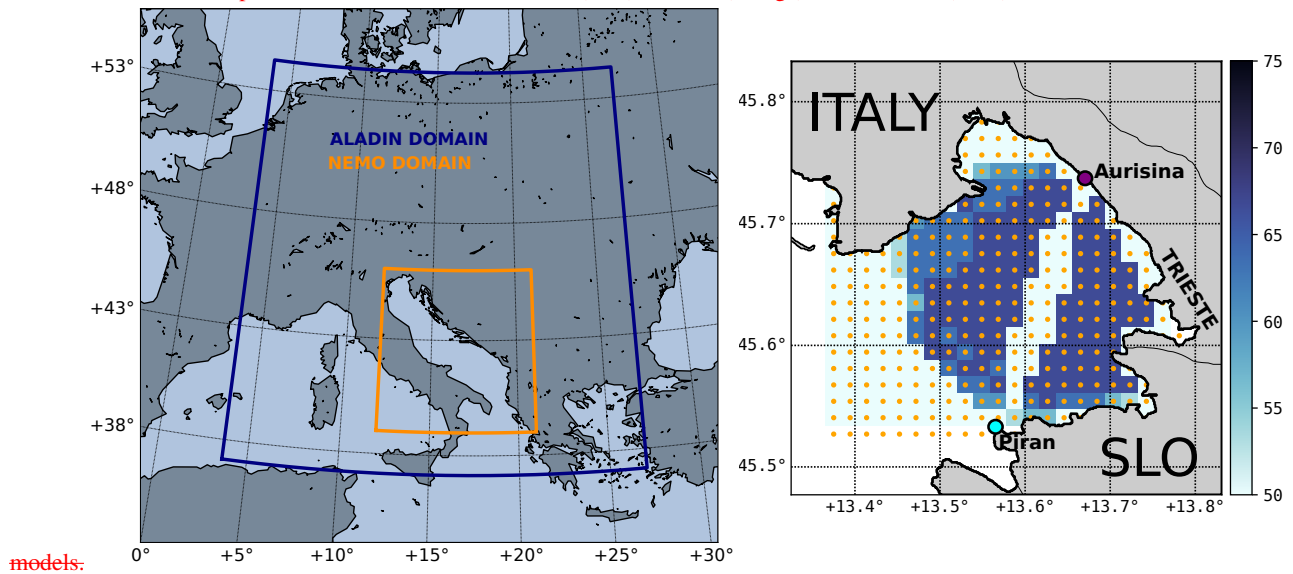
148 data assimilation as well.

Figure 3. Left: Computational domains of ALADIN SI (blue) and NEMO (orange) numerical models. Right: WERA HF radar grid (orange dots) and data availability percentage per grid point between 29 Oct 2018 16 UTC and 30 Oct 2018 21 UTC.

3.1.2 ECWAM Wave Model

The wave model used in this study is running operationally at Slovenian Weather Service. It is a regional setup of ECWAM cycle 46R1 code (full documentation is available at https://www.ecmwf.int/sites/default/files/elibrary/2018/18717-part-vii-ecmwf-wave-model) on a regular $(1°/60)$ longitude-latitude grid. Model domain spans $10° - 24°$ E and $30° - 46°$ N, see Figure 3. The model uses 25 frequency bins and 36 direction bins. Since the ECWAM domain extends south to the north African coast (to capture the swell from Central Mediterranean during Scirocco episodes), we provide wind forcing as a hybrid of ALADIN SI and ECMWF operational global forecast surface winds. ALADIN SI surface winds are used as forcing over the Adriatic basin, while ECMWF fields are used in the central Mediterranean outside of the ALADIN domain. A linear interpolation is applied over 5 cells to reduce wind gradients between the two products. It is worth noting that the ALADIN SI model is forced at the boundary by the same ECMWF product we use to provide winds to ECWAM outside (and south of) the ALADIN domain. Computational timesteps are 45 s for the propagation and 360 s for the source function. A second order propagation scheme is used. Deep water approximation is not enforced. No lateral boundary conditions are enforced at the eastern and western lateral open boundary. The latter is acceptable since the waves provided at the lateral boundaries cannot propagate into the Adriatic, which is our primary domain of interest, see Figure 3.

7

3.1.2 ALADIN Atmospheric Model

The version of the model used for the experiments in this paper is currently operational at the Slovenian Weather Service. It runs on a 432×432 horizontal Lambert conic conformal grid with 4.4 ~~km~~ km resolution and 87 vertical levels with the model top at 1 hPa and model integration time step of 180 s. The model domain spans $[0.7° \, W, 28.6° \, E]$ in longitude and $[37.4° \, N, 55.0° \, N]$ in latitude, see Figure 3. The physics package used in the model is the so-called ALARO-0, that uses Modular, Multi-scale, Micro-physics and Transport (3MT) structure (Gerard et al., 2009). Initial conditions for the model are provided by atmospheric analysis with 3 hourly three-dimensional variational assimilation (3D-Var) (Fischer et al., 2005; Strajnar et al., 2015) and optimal interpolation for surface and soil variables. Sea surface temperature (SST) in the model is initialized from the most recent host model analysis of the ECMWF model that uses Operational Sea Surface Temperature and Sea Ice Analysis (OSTIA, Donlon et al., 2012), supplied by the National Environmental Satellite, Data and Information Service (NESDIS) of the American National Ocean and Atmospheric Administration (NOAA). Information at the domain edge is obtained from the global model by applying Davies relaxation (Fischer et al., 1976). Lateral boundary conditions are provided by the ECMWF Boundary Conditions Optional project and are applied with a 1 h period in the assimilation cycle and a 3 h period during model forecasts. Boundary condition information is interpolated linearly for time steps between these times. Further details about the model setup and assimilation scheme are available in ~~Strajnar et al. (2015); Ličer et al. (2016)~~Strajnar et al. (2015, 2019); Ličer et al. (2016).

4 ~~Particle Tracking Models~~

3.1 Lagrangian Models and OpenDrift Setup

3.2 ~~OpenDrift Model and Setup~~

Lagrangian or particle tracking models are used for general purpose tracking problems from marine oil-spill dispersion modelling to water age, marine bacterial transport and object drift forecasting. Typically an arbitrary number of particles N_p (*i.e.* several thousand) are seeded at the initial location and subjected in each timestep to advection, turbulent diffusion and, if applicable, fate. Lagrangian trajectory $\mathbf{r}_p(t)$ of $p-$th particle $(p = 1, \ldots, N_p)$ is computed using a suitable numerical method (*i.e.* Runge-Kutta or Euler method) to integrate the following initial value problem

$$\frac{d\mathbf{r}_p(t)}{dt} \ = \ \mathbf{u}_c(\mathbf{r}_p(t), t) + \mathbf{l}_p(\mathbf{r}_p(t), t) + \mathbf{u}_s(\mathbf{r}_p(t), t) \tag{1}$$

$$\mathbf{r}_p(0) \ = \ \mathbf{r}_{0,p} \tag{2}$$

where t denotes time and $\mathbf{r}_{0,p}$ in Equation (2) denotes initial position of p-th particle.

Terms of the right hand side of equation (1) are as follows. Term $\mathbf{u}_c(\mathbf{r}_p(t), t)$ denotes the Eulerian ocean current at particle location $\mathbf{r}_p(t)$ at time t. In this study this term is obtained from the NEMO circulation model (Section 3.1.1) for forward propagation simulations or from WERA HF radar observations for back-propagation simulations (Section 4.1). Term $\mathbf{l}_p(\mathbf{r}_p(t), t)$ denotes leeway of p-th particle at particle location $\mathbf{r}_p(t)$ at time t. Leeway term is computed from ALADIN winds (Section

191 3.1.2) as follows. Due to lift forces on the drifting object, its leeway is not oriented strictly downwind but has a crosswind

192 component as well or $\mathbf{l} = (l_\parallel, l_\perp)$, where $l_\parallel$ and $l_\perp$ are downwind and crosswind leeway components respectively. Experimental

193 data however suggests an almost linear relationships between windspeed and downwind and crosswind leeway components

194 (Breivik and Allen, 2008). Therefore downwind leeway component can be parametrized as $l_\parallel = a_\parallel u_{10} + b_\parallel$, where u_{10} denotes

195 windspeed. On the other hand the crosswind force can point both to the left or to the right of wind, depending on the

196 orientation and shape of the object in the wind field. Therefore crosswind leeway degenerates into left-drifting crosswind

197 leeway component $l_\perp^L = a_\perp^L u_{10} + b_\perp^L$ and a right-drifting crosswind leeway component $l_\perp^R = a_\perp^R u_{10} + b_\perp^R$. Coefficients $(a_\parallel, b_\parallel)$,

198 $(a_\perp^L, b_\perp^L)$ and $(a_\perp^R, b_\perp^R)$ are determined from observations as a least square linear fit between observed wind velocity and

199 observed leeway vector (Breivik and Allen, 2008), (Allen and Plourde, 1999). The coefficients $(a_\perp^L, b_\perp^L)$ and $(a_\perp^R, b_\perp^R)$ are

200 similar but not identical. This linear regression also yields downwind, left-drift and right-drift standard deviations for each

201 fit.

202 Term $\mathbf{u}_s(\mathbf{r}_p(t), t)$ on the right hand side of the equation (1) is the Stokes drift contribution, *i.e.* orbital mean location shift

203 due to unclosed Lagrangian particle orbits in the surface gravity wave field. Note however that since coefficients $(a_\parallel, b_\parallel)$

204 and $(a_\perp, b_\perp)$ are determined from observations, they already contain the Stokes drift contribution in the observed leeway.

205 If one attemps to model object's leeway using downwind and crosswind leeway coefficients based on empirical data from

206 (Allen and Plourde, 1999), Stokes drift term must be omitted from the initial value problem (1)-(2).

207 OpenDrift is an open-source Python-based Lagrangian particle modelling code developed at the Norwegian Meteorologi-

208 cal Institute with contributions from the wider scientific community. ~~It is described in detail in Dagestad et al. (2018). It~~ Its

209 Leeway() module implements leeway computation in the fashion described in the previous paragraph, for further details see

210 Breivik and Allen (2008) and Dagestad et al. (2018). Apart from leeway computations OpenDrift supports a wide range of of-

211 fline (~~i.e.~~ *i.e.* with precomputed currents and winds) predictions from oil spills and drifting objects to microplastics and fish

212 larvae transport. Particle seeding is very convenient to use and its Leeway module supports a wide range of object types with dif-

213 ferent lift and drag behaviour under current and wind forces (Dagestad et al., 2018). ~~Object drift is decomposed into downwind~~

214 ~~and crosswind components (Breivik and Allen, 2008) based on empirical observations collected in Allen and Plourde (1999).~~

215 The object types used in this study were of two ~~types~~kinds that we believe are most adequate for leeway modeling in

216 this particular case. First drift object type was Person-in-water~~(PIW-1)~~, corresponding to empirically determined (Allen and

217 Plourde, 1999) downwind slope of ~~1.93 %~~$a_\parallel = 1.93\%$, downwind standard deviation of 0.083 ~~m s~~ms^{-1}, right slope of ~~0.51~~

218 ~~%~~$a_\perp^R = 0.51\%$, right standard deviation of 0.067 ~~m s~~ms^{-1}, left slope of ~~-0.51 %~~ $a_\perp^L = -0.51\%$ and left standard deviation of

219 0.067 ~~m s~~ms^{-1}.

220 Second object type was ~~PERSON-POWERED-VESSEL-2 (Surf board with person~~ Person-Powered-Vessel-2 (person with

221 surf board), corresponding to empirically determined (Allen and Plourde, 1999) downwind slope of ~~0.96 %~~$a_\parallel = 0.96\%$, down-

222 wind standard deviation of 0.12 ~~m s~~ms^{-1}, right slope of ~~0.54 %~~$a_\perp^R = 0.54\%$, right standard deviation of 0.094 ~~m s~~ms^{-1}, left

223 slope of ~~-0.54 %~~ $a_\perp^R = -0.54\%$ and left standard deviation of 0.067 ~~m s~~ms^{-1}~~).~~.

224 The simulation was run in both cases for ~~31~~ 48 hours using a second order Runge-Kutta scheme. Forcing data consisted of
225 NEMO currents and ALADIN SI 10m winds from the 00 UTC operational runs of both models, performed on 29 Oct 2019 at
226 ~~the Slovenian Environment Agency~~ARSO.

3.2 ~~FlowTrack~~ Model and Setup

228 ~~FlowTrack is an offline individual-based Lagrangian tracking model, developed for the general purpose tracking problems~~
229 ~~from marine oil-spill dispersion modelling to water age, marine bacterial transport and object drift forecasting. The model was~~
230 ~~written by one of the authors (M. L.) in Fortran 95 with shared memory (openMP)parallelization. An arbitrary number of~~
231 ~~particles N_p (i.e. several thousand) are allowed. In this study $N_p = 408$ particles were seeded in a 1 km $\times$1 km square around~~
232 ~~the initial location. Once the particle is initialized in the wet cell of the model grid, it is subjected in each timestep to advection,~~
233 ~~turbulent diffusion and, if applicable, fate. Lagrangian trajectory $\mathbf{r}_p(t)$ of p-th particle ($p = 1, \ldots, N_p$) is computed using a~~
234 ~~second order Runge-Kutta method (Euler method is also available) to integrate the following initial value problem~~

235 $$\frac{d\mathbf{r}_p(t)}{dt} \equiv \mathbf{u}_c(\mathbf{r}_p(t), t) + q \cdot \mathbf{u}_{w,p}(\mathbf{r}_p(t), t) + \mathbf{u}_s(\mathbf{r}_p(t), t) + \mathbf{u}'$$

236 $$\mathbf{r}_p(0) \equiv \mathbf{r}_{0,p}$$

237 ~~where $\mathbf{r}_{0,p}$ in Equation (2) denotes initial position of p-th particle.~~ At the time of the incident however, OpenDrift was not
238 implemented at ARSO and could not be used. Due to the incident, the pipeline of input data preparation and a specific drifter
239 type OpenDrift computation was developed and is now available to forecasters at ARSO as an internal web service. With
240 ALADIN SI and NEMO fields (pre)computed operationally, subsequent on-demand OpenDrift simulations take under ten
241 minutes to complete.

242 ~~Terms of the right hand side of equation (1) are as follows. Term $\mathbf{u}_c(\mathbf{r}_p(t), t)$ denotes the Eulerian current at particle location~~
243 ~~$\mathbf{r}_p(t)$ at time t. This term is obtained from the NEMO circulation model. Term $\mathbf{u}_{w,p}(\mathbf{r}_p(t), t)$ denotes the wind drift vector of~~
244 ~~the p-th particle at particle location$\mathbf{r}_p(t)$ at time t. Wind drift generally has lift and drag component, thus deviating from~~
245 ~~the wind direction. This deviation is treated in FlowTrack by rotating the wind drift vector of p-th particle by an angle~~
246 ~~$\theta(p) \in [-L_\alpha, +L_\alpha]$, where L_α stands for the leeway divergence angle (Allen and Plourde, 1999). In this work L_α was set~~
247 ~~to 20° as recommended for a person with surfboard in Table 8-1 of Allen and Plourde (1999). Since wind lift can generally act~~
248 ~~to the left or to the right of wind, with both options having equal probabilities (Breivik and Allen, 2008), FlowTrack distributes~~
249 ~~$\theta(p)$, where $p = 1, \ldots, N_p$, linearly over the $[-L_\alpha, +L_\alpha]$ interval, namely~~

250 $$\theta(p) = -L_\alpha + \frac{p-1}{N_p - 1} \cdot 2L_\alpha.$$

251 ~~Each particle retains its respective angle of rotation throughout the simulation and does not jibe. The wind drift vector of the~~
252 ~~p-th particle is then computed from ALADIN SI 10m winds $\mathbf{u}_{10}(\mathbf{r}_p(t), t)$ at particle location as~~

253 $$\mathbf{u}_{w,p}(\mathbf{r}_p(t), t) = \begin{bmatrix} \cos\theta(p) & -\sin\theta(p) \\ \sin\theta(p) & \cos\theta(p) \end{bmatrix} \cdot \mathbf{u}_{10}(\mathbf{r}_p(t), t).$$

254 ~~Parameter q in equation (1) scales the object's drift speed to the wind speed. It was estimated from OpenDrift empirical~~

255 ~~coefficients mentioned in the previous sections as follows. Downwind drift scales as $q_{DW} = 1.93$ % of the wind speed.~~

256 ~~The downwind standard deviation is 0.083 m s^{-1}, which at 15 m s^{-1} (i.e. typical wind speed during the event) amounts~~

257 ~~to $q_{DW}^\sigma = 0.4$ %. The crosswind components in OpenDrift scale as $q_{XW} = 0.51$ % of the windspeed, with standard deviations~~

258 ~~of 0.067 m s^{-1}, which at 15 m s^{-1} amounts to $q_{XW}^\sigma = 0.34$ %. Since mere rotation of the wind drift vector, applied in~~

259 ~~FlowTrack, does not alter its modulus, and hence disregards the wind lift force, we attempted to compensate for this by~~

260 ~~estimating $q = \sqrt{(q_{DW} + q_{DW}^\sigma)^2 + (q_{XW} + q_{XW}^\sigma)^2} \approx 2.5$ percent of the wind speed.~~

4 Results and Discussion

262 ~~Term $\mathbf{u}'$ in (1) represents random fluctuations in the velocity vector to simulate subgrid turbulent diffusion. In the present paper,~~

263 ~~the modulus of fluctuations has been manually constrained to $2 \cdot 10^{-2}$ m s^{-1}. Term $\mathbf{u}_s(\mathbf{r}_p(t), t)$ on the right hand side of~~

4.1 Drift Trajectory Verification using Back-propagation with HF Radar Currents

265 As noted above, survivor had no GPS or watch to keep track of his movements in space and time. Therefore his reconstruction

266 of the drift trajectory is burdened with error. What is known however is the ~~equation (1) is the Stokes drift contribution,~~

267 ~~i.e. Eulerian mean of unclosed Lagrangian particle orbits in the surface gravity wave field. It was however shown (see~~

268 ~~(Hackett et al., 2006; Breivik and Allen, 2008) for further references) that Stokes drift, while present in the motion of the water,~~

269 ~~has negligible impact on driftspeed of objects whose typical dimension is more than roughly six times smaller than surface~~

270 ~~gravity wave wavelength λ_w. We can compute λ_w from surface gravity wave dispersion relation $\omega(k) = \sqrt{gk\tanh(kH)}$. Since~~

271 ~~wave vector is $k = 2\pi/\lambda_w$, we can solve for λ_w by iterating~~

272
$$\lambda_w = \frac{gT_w^2}{2\pi}\tanh\frac{2\pi H}{\lambda_w}$$

273 ~~where T_w is the mean wave period of the wave field obtained from the ECWAM model at a representative point along the~~

274 ~~particle trajectory during the 29~~ exact location and time of his beaching: a beach in Sistiana (Italy) on 30 Oct ~~2018 storm, g~~

275 ~~is~~acceleration ~~due to gravity and H is the undisturbed ocean depth. Within the drifting area surface gravity wave wavelengths~~

276 ~~during the~~ 2018 at 16 UTC. HF radar surface current measurements cover only the final part of the drift domain. They can

277 therefore not be used for the forward-propagation simulation starting at the accident location, but they can nevertheless be

278 employed to perform Lagrangian back-propagation (upwind and upstream advection backwards in time) starting from the

279 beaching location.

280 This simulation is of course limited to the HF system domain, described in section 2.2, but it should offer some insight

281 into the final part of the drift trajectory and serve as an independent check of survivor's trajectory estimate. To this end, HF

282 radar currents over the period of the drift were first gap-filled in space using nearest-neighbor interpolation and then gap-filled

283 in time using linear interpolation. Wind component for back-propagation was provided by the ALADIN atmospheric model

284 (see section 3.1.2) and remapped to HF radar grid in space and time. OpenDrift code was used to perform back-propagation
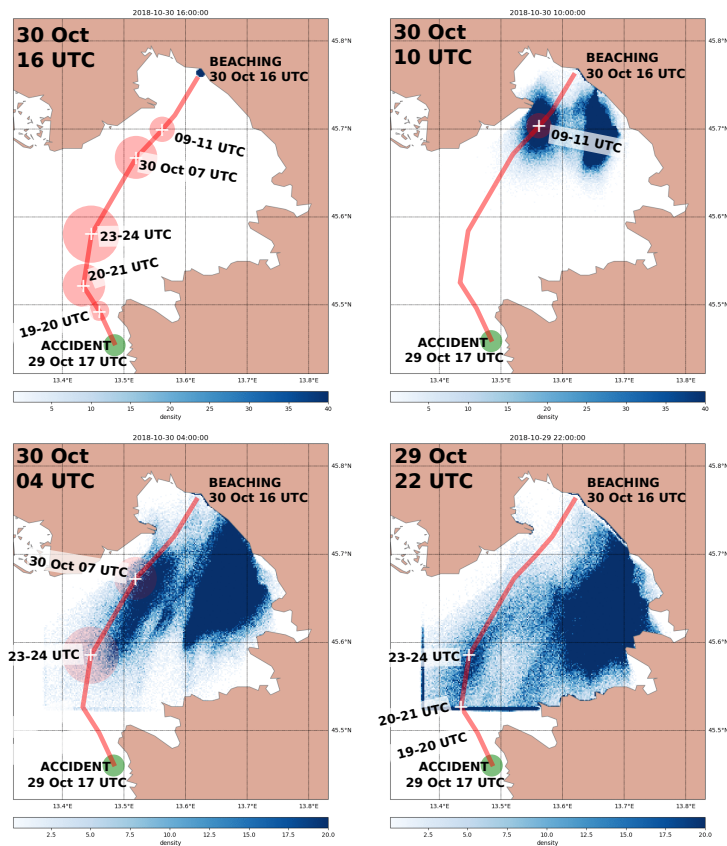
Figure 4. Temporal back-propagation of virtual drifters from beaching location using HF radar measurements and ALADIN winds as inputs for OpenDrift model. Back-propagation starts at beaching location (top left panel). Particle spatial density is shown every six hours of the simulation, as denoted by timestamps in top left corner of each panel. Red line and superimposed dates are survivor's estimates of his trajectory (for clarity, only relevant timesteps of survivor's reconstruction are shown in each panel). Transparent red circles denote survivor's estimate of the error in his location at stated time. Dark blue straight lines in the bottom right panel, appearing along the southwest corner of HF radar computational domain, result from accumulation of particles which cease to advect when they reach the outer limits of the HF radar domain.

simulation and results are presented as particle numeric density per area, in similar fashion as in (Röhrs et al., 2018; Dugstad et al., 2019). To ensure smooth maps of particle density, a large number (fifty thousand) of virtual particles of type "person with surf board" were released at the beaching location at beaching time and advected backward in time in 12-minute timesteps (0.2 hours) for 18 hours. Results of these simulations are depicted in Figure 4, which shows particle density per density cell area. Density cells over which the particles are counted, were chosen to be of 150 m $\times$ 150 m dimensions. This 10-fold reduction in cell computation area was done because the original HF radar grid (1500 m $\times$ 1500 m, see Figure 3) is too coarse to produce smooth maps of particle density.

292 Figure 4 indicates two distinct pathways to Sistiana during the time of the drift: firstly we have the southern branch arriving
293 to the beaching site from the region south-southeast of the beaching site. Secondly, a northwestern branch of propagation is
294 visible roughly along the survivor's trajectory estimate. The northwestern pathway is, to a large degree, spatially and temporaly
295 consistent with the survivor's trajectory. Survivor's estimates of his location on 29 Oct ~~2018 storm exceeded 50-70 m. Since~~
296 ~~the surfboard is roughly 3 m long, Stokes drift effect can be safely ignored, which simplifies initial value problem (1)-(2) to~~

297
$$\frac{d\mathbf{r}_p(t)}{dt} \equiv \mathbf{u}_c(\mathbf{r}_p(t),t) + q \cdot \begin{bmatrix} \cos\theta(p) & -\sin\theta(p) \\ \sin\theta(p) & \cos\theta(p) \end{bmatrix} \cdot \mathbf{u}_{10}(\mathbf{r}_p(t),t) + \mathbf{u}'$$

298 $\mathbf{r}_p(0) \equiv \mathbf{r}_{0,p}.$

299 ~~In situations where Stokes drift is not negligible, FlowTrack is currently adapted for use with Stokes drift field from ECWAM~~
300 ~~cycle 46R1, but generalization to any other wave model whose Stokes drift results can be remapped to a regular longitude-latitude~~
301 ~~grid is trivial. Forcing data to FlowTrack is identical to the one of OpenDrift, and consisted of NEMO currents and ALADIN~~
302 ~~SI 10m winds from the 00 UTC operational runs of both models, performed on 29~~ 22 UTC and 30 Oct ~~2019 at the Slovenian~~
303 ~~Environment Agency~~10 UTC agree well with the computed virtual particle density maps. During the night, when survivor
304 reported feeling maximum distress, the back-propagation estimate of trajectory is located a mile or two to the east of his
305 reconstruction.

306 ## 5 ~~Results and Discussion~~

307 ### 4.1 Marine Conditions from Observations and Models

308 In this section we present a qualitative analysis of marine conditions from available observations, and also marine drift results
309 from both particle tracking models presented in Section 3.1.
310 ~~HF radar measurements in the Gulf of Trieste during the period of the drift. Since there are gaps in surface current~~
311 ~~measurements, the closest observations to 29 Oct 22 UTC and 30 Oct 04, 10, 16 UTC are depicted. NEMO currents were~~
312 ~~bilinearly interpolated to WERA grid points. Arrow lengths from both fields are commonly scaled.~~
313 Figure 5 depicts wind measurements and ALADIN SI modelled winds at the Vida coastal buoy (12 ~~km~~ km northeast of the
314 accident location, see Figure 1 b).) for the timewindow 29 - 31 Oct 2019. Qualitatively there is a very solid agreement between
315 the two timeseries. Measured wind at Vida exhibits southeasterly 140° direction in the hours after the accident (left dashed line
316 in Figure 5), followed by a shift to slight south-southwest 190° between 30 Oct 00 UTC and 04 UTC, and finally a southerly
317 180° direction during the day ~~. (All~~ (all directions in the paper are stated in nautical notation, ~~i.e.~~ i.e. 0° marking north, 90°
318 marking east.) Wind speed is constantly around 15 - 20 ~~m s~~ms^{-1}.
319 HF observations in Figure 6 are presented as a qualitative check for the NEMO model surface currents during the 24 hours
320 of the drift. HF measurements and modeled currents both exhibit eastward topographically constrained coastal current in the
321 northern part of the Gulf between Grado and Soča/Isonzo rivermouth, with NEMO tending to underestimate observations (as
322 shown below however, wind drift was the main contribution to the drift). Absence of the coastal current on Oct 29th 22 UTC
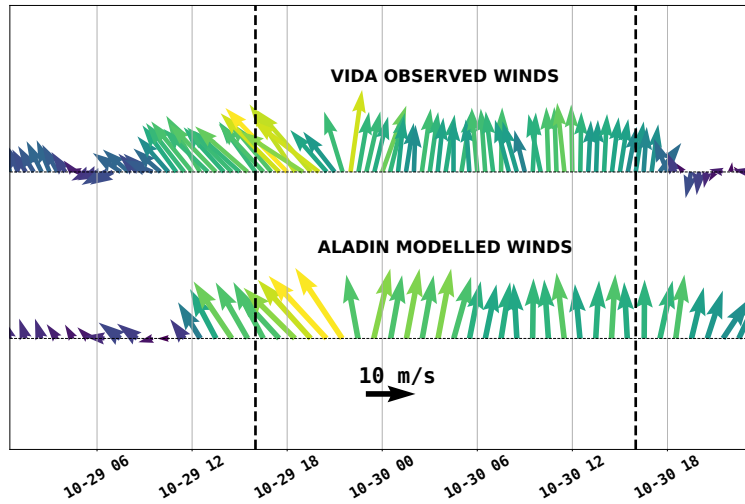
Figure 5. Arrow plots of observed and ALADIN SI modelled wind directions at Vida coastal buoy during 29 Oct 2018 event. Drift period is marked with dashed vertical lines. Arrows are colored by their wind speed.
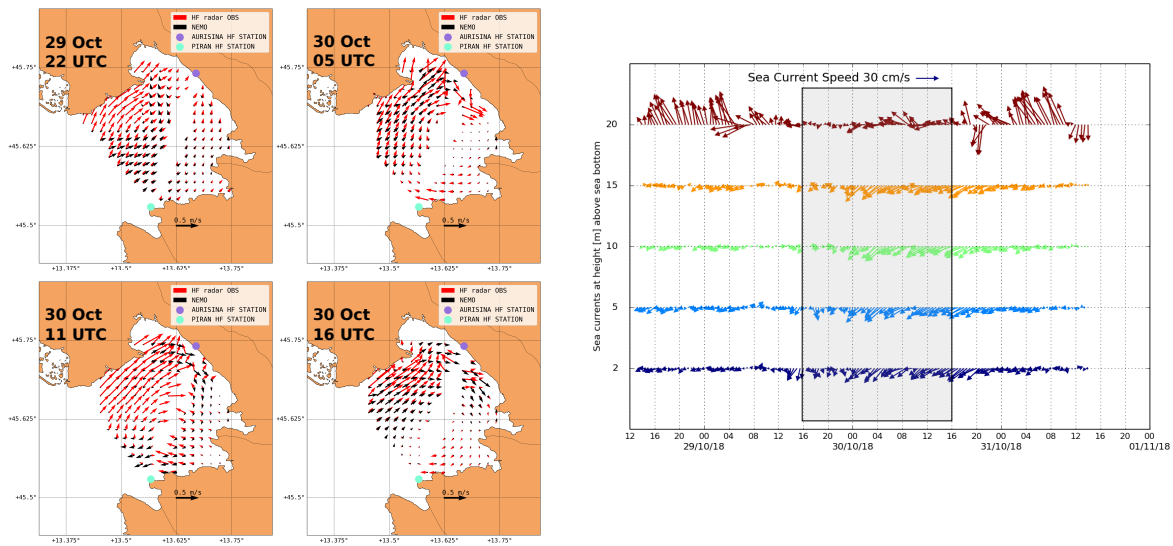

Figure 6. Left: HF radar measurements in the Gulf of Trieste during the period of the drift. Since there are gaps in surface current measurements, the closest observations to 29 Oct 22 UTC and 30 Oct 04, 10, 16 UTC are depicted. NEMO currents were bilinearly interpolated to WERA grid points. Arrow lengths from both fields are commonly scaled. Right: Arrow plot of ADCP measurements of ocean currents at Vida coastal buoy during 29 Oct 2018 event (shaded rectangle delimits the time window of the drift). Surface current timeseries is plotted in the top line.

323　might be related to the model treatment of high Soča/Isonzo discharge, which in itself generates westward inertial current in

324　that part of the modelling domain, and might be counteracting wind driven (eastward) currents. Verification of the NEMO

325　model versus ten months of hourly HF radar currents (not shown in detail in this paper) yields a bias in zonal velocity between

326　0 and -2.5 cms^{-1} and a bias between +2.5 and -2.5 cms^{-1} for meridional velocity. NEMO model underestimations during

327　the limited period of this case study were unfortunately much larger: spatially averaged (over the HF domain) and temporaly

328　averaged (over the period of the drift) NEMO biases amounted to -6.3 cms^{-1} for zonal velocity and a bias of -9.2 cms^{-1} for

329　meridional velocity. NEMO setup therefore exhibited below-average performance during the period of interest. This will have

330　to be further addressed as a separate issue and needs to be kept in mind when interpreting results below. On the other hand both

331　the model and the HF measurements ~~indicate~~ exhibit an inflow over most of the surface area of the Gulf which indicates that

332　the surface layer on Oct 29th 22 UTC was wind dominated, ~~exhibiting an inflow over most of the surface area of the Gulf,~~ see

333　also (Malačič et al., 2012).

334　　Another common feature of NEMO currents and HF radar observations is the general anticyclonic character of the surface

335　circulation through the rest of the night and the following day. This is in contrast with the Northern Adriatic basin-scale cyclonic

336　current pattern during Scirocco episodes (not shown) and stems from the fact that Scirocco induced surface currents, flowing

337　north along the Istrian coast, typically branch upon hitting the northern end of the Adriatic basin. The eastward branch of this

338　wind driven current inflows into the Gulf of Trieste along the northern coastline. Such inflow, visible in modeled and observed

339　currents is therefore not unexpected during Scirocco episodes. As is further shown in ~~Figure ??~~ the right panel of Figure 6, *in*

340　*situ* currents measured at Vida buoy also exhibit a westward direction over the entire water column during the timewindow

341　of the drift, and are therefore consistent with the overall anticyclonic character of the surface circulation, exhibited in the

342　model and radar surface current maps. ~~NEMO model underestimation of the observed surface currents will however need to~~

343　~~be thoroughly addressed in further investigations.~~

344　　Figure 7 depicts current and wind drift inputs to both models over the period of the windsurfer's drift.The wind drift seems to

345　be the dominant driving factor of the windsurfer's drift, its speed being roughly double that of the surface currents. Wind drift

346　prior to (not shown) and at 22 UTC has a clear southeasterly direction (at Umag - offshore) at roughly 140-160°, consistent

347　with the windsurfer's experience and his inability to reach Savudrija in time. During the night the wind direction shifts into a

348　south-southwesterly to about 190°, also consistent with his experience. In the morning of 30 Oct 2018 and through the day,

349　the wind direction is predominantly southern at 180°. This is all in agreement with the direction shift measured at Vida buoy

350　(Figure 5).

351　~~OpenDrift simulation of the Person in Water (PIW-1) object type. Lagrangian drift is depicted every 6 hours after the accident~~

352　~~(green dots mark the initial seeding location) on 29 Oct 2019 16 UTC. Red line denotes trajectory of the drift, as reconstructed~~

353　~~by the survivor. White crosses denote locations at specific times, while red circles around crosses denote uncertainty estimates~~

354　~~of the respective location estimates.~~

355　　NEMO currents at 22 UTC indicate northward direction along the coast of Istria and also a surface inflow along all but

356　the northernmost part of the opening of the Gulf of Trieste. The northernmost part along the northern coast of the Gulf most
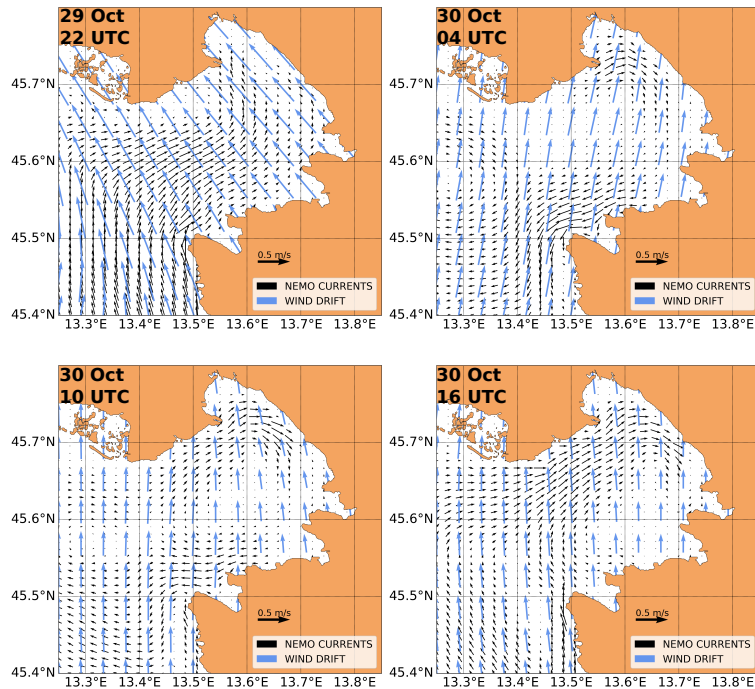
Figure 7. 6-hourly same-scale snapshots of NEMO currents (black arrows) and ALADIN SI 10m wind $\mathbf{u}_{10}$ induced wind drift (blue arrows) over the period of the windsurfer's drift. Only purely downwind arrows with no ~~crosswind~~ departure from the ALADIN SI wind velocity ~~vector~~ direction are plotted, computed as $a_{\parallel}\mathbf{u}_{10}$ using OpenDrift "person in water" downwind slope $a_{\parallel} = 1.93$ %. Only every third wind point is plotted for clarity. Arrow lengths from both fields are commonly scaled and both arrow length units are $\mathrm{m\,s^{-1}}$.

357 likely shows no notable inflow due to inertial westward coastal current from the Soča/Isonzo river, which manifests itself as an
358 outflow from the Gulf, confined to this part of the coast (see Figure 1 for the related river plume).

4.2 Lagrangian simulation results

360 In this section we present OpenDrift simulations with NEMO model current inputs and ALADIN SI 10m wind inputs during
361 19 Oct 2018 16 UTC and 30 Oct 2018 16 UTC. Simulations were performed running forward-propagation in time, starting
362 particle drift from the accident location at Oct 2018 16 UTC.
363   OpenDrift results for drifting object type ~~Person in Water (PIW-1)~~ "person in water" are presented in Figure 8. Figure shows
364 6-hourly snapshots of ~~particles~~particle densities (number of particles per cell area), initially seeded in the green region at 29 Oct
365 2019 16 UTC. To ensure smooth maps of particle density, a large number (fifty thousand) of virtual particles of type "person in
366 water" were released at the accident location at accident time and advected forward in time in 12-minute timesteps (0.2 hours)
367 for 24 hours. Cells over which the particles are counted were again chosen to be of 150 m $\times$ 150 m dimensions. This reduction
368 in cell computation area was again done because the original NEMO grid resolution (1000 m $\times$ 1000 m) is too coarse to
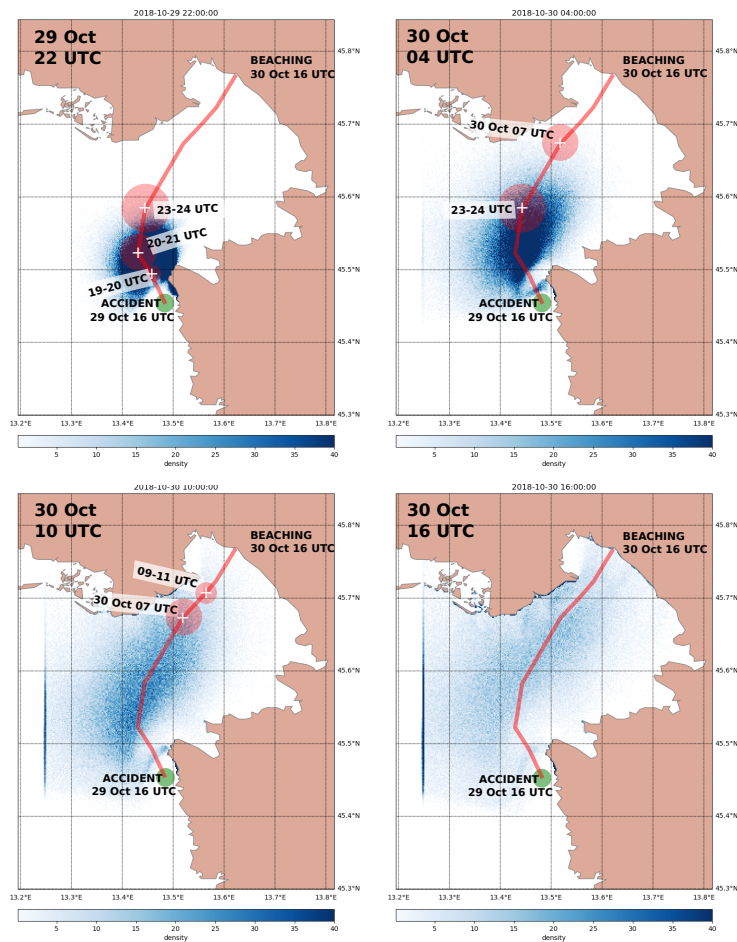
16

Figure 8. Lagrangian particle density [number of particles per cell area] from OpenDrift simulation of the ~~PERSON-POWERED-VESSEL-2~~ "person in water" object type. Lagrangian simulation drift is depicted every 6 hours ~~after the accident~~ (~~green dots mark~~ indicated by a timestamp in the ~~initial seeding location~~upper left corner of each panel) after the accident on 29 Oct 2019 16 UTC. Red line denotes ~~trajectory of the~~ drift ~~,~~trajectory as reconstructed by the survivor. White crosses and time inserts denote locations ~~at specific~~ and times from survivor's trajectory estimate, while red circles around crosses denote survivor's uncertainty estimates of the respective location~~estimates~~.

369 produce smooth maps of particle density. After 6 ~~hours, at 22 UTC, roughly 75 percent of particles are still in the watercolumn,~~
370 ~~with the majority of the particles lagging behind the estimated windsurfer location . Particles at the northern forefront seem~~
371 ~~however to be well in the region of where the windsurfer estimated his position between 20 UTC and 23 UTC. The search and~~
372 ~~rescue area after 6~~ hours~~amounts to estimated 70 km² (this estimate is made by computing the area of a polygon, determined~~
373 ~~by locations of the outermost group of particles)~~, at 22 UTC, the set of the particles envelops the estimated windsurfer location
374 but the center of gravity of the particle set is lagging southeast of survivor's estimated location.

Shift in the wind direction from southeast to south-southwest (see Figure 5), occuring sometime after 29 Oct 22 UTC and lasting until 04 UTC, causes a corresponding shift in particles' drifting directions ~~. The envelope of particles' trajectories fully contains the reconstructed trajectory . The search and rescue area after 12 hours amounts to roughly 240 km^2~~ and a stretched dispersal of the particle set along the survivor's trajectory estimate.

First particles are beaching on the northern shore of the Gulf between 04 UTC and 10 UTC. This predominantly occurs between Grado and the Soča/Isonzo river mouth. Particles in the Gulf are propagating along the reconstructed trajectory, but with increasing lateral and axial extent~~: search and rescue area after 18 hours amounts to estimated 500 km^2.~~. At 10 UTC the set is dispersed over northwestern half of the Gulf of Trieste and are stretched roughly along the survivor's trajectory. While majority of particles lag behind the survivor's estimated location the set does extend over survivor's estimated location which is enveloped by the forefront of the particles set.

After 24 hours ~~several (>10) particles beach~~ the particles set is almost homogeneously dispersed over the northwestern half of the Gulf, with some of the particles beaching within 2 ~~km~~ km of the actual beaching location. ~~Search and rescue area at this point consists of most of the Gulf of Trieste, covering 650 km^2.~~

OpenDrift results for drifting object type ~~PERSON-POWERED-VESSEL-2 (Surf board with person)~~ "person with surf board" are presented in Figure 9. After 6 hours, at 22 UTC, ~~roughly 90 percent of particles are still in the water column, with the majority of the particles centered around the estimated windsurfer location . After 12 hours, at 04 UTC , the envelope of the particles seems to be lagging a few hours behind - they are centered at the 23-24UTC estimate of the surfers position. The forefront~~ the set of the particles envelops the estimated windsurfer location and the center of gravity of the particle set is closer to the survivor's estimated location than in the "person in water" case. This particle set is also overlapping with the higher density region of the northernwestern pathway from HF radar currents back-propagation simulation result at 29 Oct 2018 22 UTC presented in the bottom right panel of Figure 4.

Shift in the wind direction from southeast to south-southwest (see Figure 5), occuring sometime after 29 Oct 22 UTC and lasting until 04 UTC, again causes a corresponding shift in particles' drifting directions but the dispersal of the particle ~~distribution however contains the estimated trajectory at all times. The search and rescue area after 6 hours amounts to estimated 45 km^2 (this estimate is made by computing the area of a polygon, determined by locations of the outermost group of particles). The search and rescue area after 12 hours in this case amounts to roughly 160 km^2.~~

~~First particles are beaching on the northern shore of the Gulf between~~ set along the survivor's trajectory estimate is somewhat lesser than in the "person in water" case. At 04 ~~UTC and~~ UTC the majority of the particles is lagging behind (*i.e.* is mostly located southwest of) both survivor's location estimate and also behind the densest region from the northwestern branch of the back-propagation simulation (bottom right panel in Figure 4). This is consistent with the fact that NEMO modelled currents are underestimating HF radar measurements used for back-propagation simulations.

At 10 ~~UTC. This predominantly occurs~~ UTC the particle set is dispersed between Grado and ~~the~~ Soča/Isonzo ~~river mouth. Particles in the Gulf are propagating along the reconstructed trajectory, but with increasing lateral and axial extent: search and rescue area after 18 hours amounts to estimated 250 km^2.~~ rivermouth, again lagging behind both survivor's location estimate
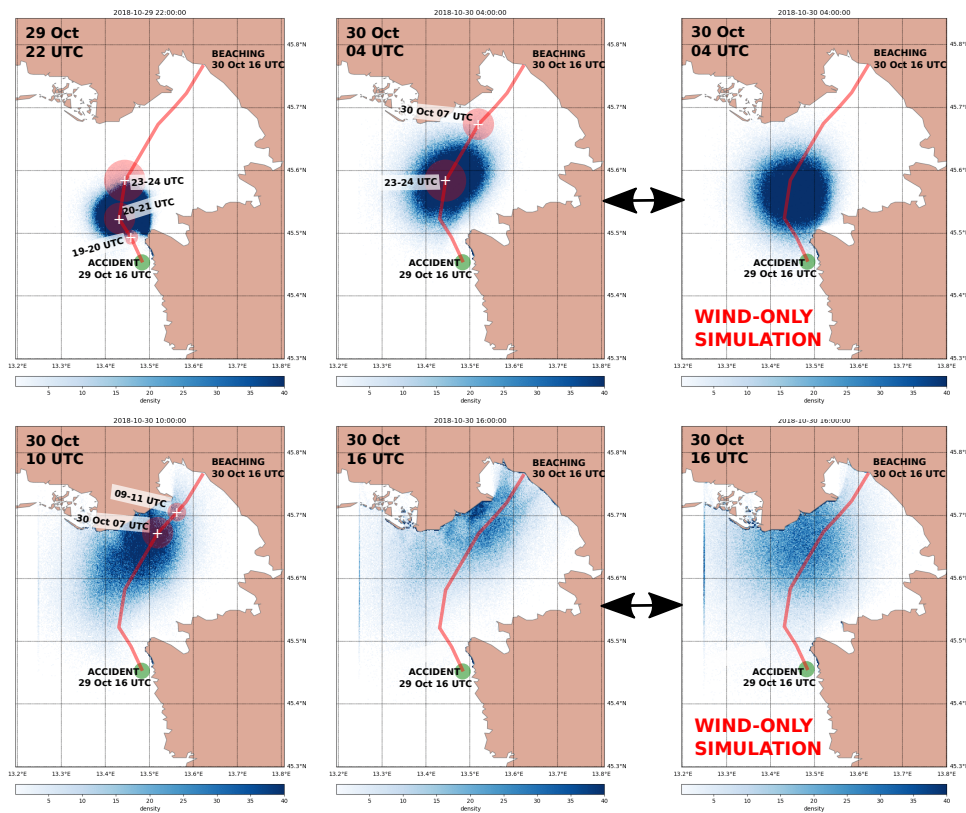
Figure 9. Same as Figure 8 ,but for ~~a FlowTrack simulation of the windsurfer's drift~~"person with surf board" object type. ~~Location of harness recovery is marked~~ Rightmost column depicts simulation results with ~~a red circle at~~ wind-only input (~~13.48 E, 45.6 N~~ and ocean currents set to zero) after 12 hours and 24 hours of the drift.

409 and the northwestern branch of the back-propagation simulation (top right panel in Figure 4). When compared to "person in
410 water" scenario, this particle set is however more clearly localized along the northern shore of the Gulf.

411 After 24 hours ~~several (>10) particles beach~~ the particles set is densest around the Soča/Isonzo rivermouth, but with a
412 clearly visible streak of particles beaching within 2 ~~km~~ km of the actual beaching location. ~~Search and rescue area at this~~
413 ~~point consists of the northern half~~ This higher localization represents some improvement over the entire northwestern half
414 ~~of the~~ of the Gulf of Trieste, ~~covering 380 km²~~ indicated by "person in water" simulation. In any case a quantitative comparison is
415 performed below to further elucidate performances of both drift simulations.

416 ~~Simulations using object type PERSON-POWERED-VESSEL-2 yield smaller SAR areas which are more consistent with~~
417 ~~the survivor's trajectory estimate than SAR areas based on PIW-1 object type. While one can clearly benefit from using the~~
418 ~~most appropriate drift parametrization, lack of information during an actual event often complicates the decision on which~~
419 ~~parametrization to use~~ Figure 9 contains also a third separate column which depicts results of a wind-only simulation (with
420 ocean currents artifically set to zero) after 12 hours and 24 hours of drift, *i.e.* at 30 Oct 04 UTC and 16 UTC respectively.

19
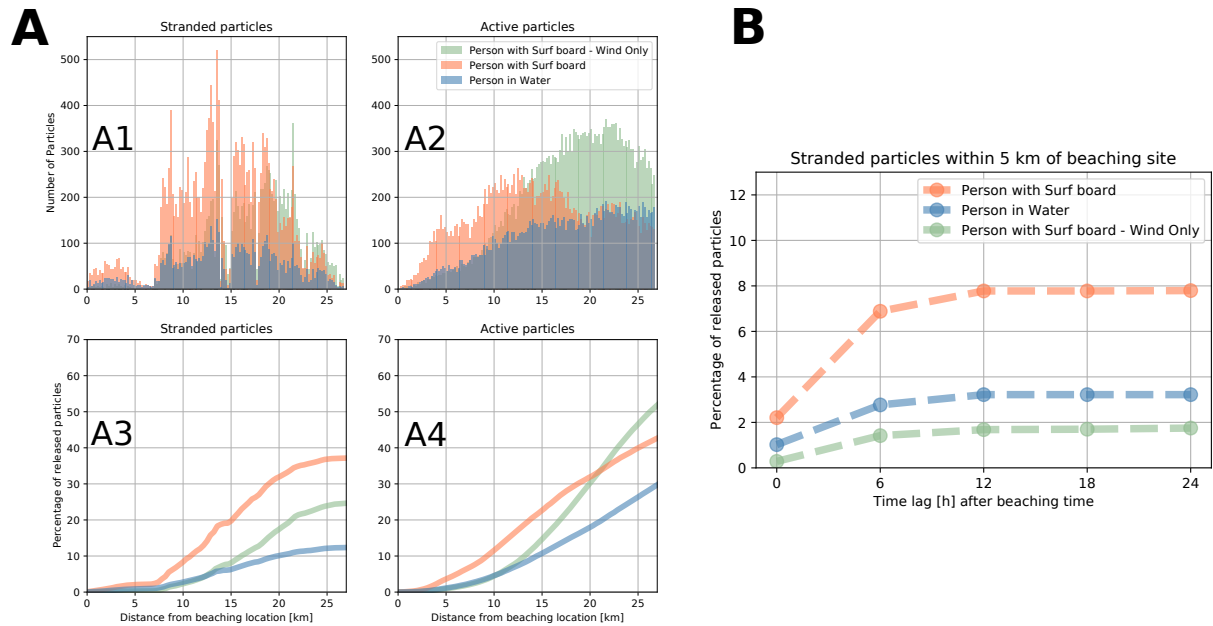
Figure 10. A. Stranded and active (right panel) particle distribution over distances from the beaching location at beaching time. B. Time dependence of acummulated percentage of particles within 5 km of the beaching site.

Comparison with the first two columns (depicting full simulations with both winds and currents) demonstrates ocean current influence to particle dispersal. Under rather homogeneous wind conditions (see Figure 7) particle dispersal due to wind is highly isotropic throughout the simulation period. Being highly inhomogeneous itself, ocean current pattern in the Gulf adds asymmetry to the wind dispersal pattern. This effect elongates somewhat the slick of particles and advects them further along the Italian coast closer towards Sistiana.

~~Simulation results from FlowTrack model are presented in Figure ??. One shortcoming of this model is immediately clear: the model currently lacks properly calibrated, object dependent diffusion both in~~ Given available data (or lack thereof) a quantitative comparison between the drift simulations can only be based on the beaching point, which is known. To pursuit this we calculated the distribution of stranded and active (non stranded, still in the water column) particles and plotted its histogram over distances from the beaching location at beaching time and also 6, 12, 18 and ~~across the propagation direction. Particles (initially seeded in a rectangular region around the accident location) consequently spread mostly laterally due to the variability in leeway divergence angle $\theta(p)$. With wind drift being the dominant factor, the overall envelope of particle trajectories correlates with the one from OpenDrift, but with somewhat narrower lateral extent. Consequently, and unlike OpenDrift, FlowTrack can at present give no useful quantitative estimate of the search and rescue area.~~

~~The simulation trajectory is also temporally consistent with the reconstructed trajectory~~ 24 hours after the beaching time. Distributions at beaching time and particle accumulation after the beaching time are depicted in Figure 10.

Panel A2 in Figure 10 indicates that at beaching time the distribution maximum of active "person with surf board" drifters is positioned about 12 km from the beaching site. It is also positioned 15 km closer to the beaching point than the distribution maximum of "person in water" drifters. This indicates a) better performance of "person with surf board" drifters, and b) a time lag in the movement of all types of drifters. As mentioned above, this is very likely due to the NEMO model surface current underestimation (of HF currents) during the event - ~~particles in the vicinity to the reconstructed trajectory do not significantly lag or overtake windsurfer's location estimate . The reconstructed trajectory is however located more or less on the eastern outer edge of all simulated routes and represents more of an outlying scenario than in the case of OpenDrift~~ this claim is further backed by the fact that WERA HF back-propagation simulations in section 4.1 seem temporaly consistent with survivor's estimate (Figure 4) and show little lag after 18 hours of the drift.

These conclusions are also implied by the particle distributions in Figures 8 and 9: at beaching time, "person in water" particles are dispersed over a much wider area than those of "person with surf board" type. Panel A2 of Figure 10 reflects that.

However, and regardless of this lag, when focusing on the accumulation of stranded particles (panels A3 and B of Figure 10), we see that at beaching time about twice as many "person with surf board" drifters stranded within 5 km of the beaching point than those of "person in water" type. The same holds for particles stranding within 10 km radius. Within 20 km radius this ratio triples. These results quantitatively substantiate claims of better performance of the "person with surf board" drifter type for this case study.

Panel B on Figure 10 shows percentage of stranded particle within 5 km distance of the beaching site in the hours after the beaching. This percentage saturates on the scale 6 hours, giving us an estimate for the time lag.

We conclude this section with a brief comment on wind-only simulations with "person with surf board" type. These simulations under homogeneous wind conditions exhibit highly isotropic spatial dispersion of particles, unlike the two scenarios which take into account ocean currents. This leads to slower accumulation of particles within 5 km radius of the beaching point (panels A3 and B of Figure 10). At these distances and by this metric, wind-only simulations are the worst performer of all three. Without putting too much weight on wind-only simulation - this does indicate the importance of topographically constrained ocean currents in semi-enclosed basins like the Gulf of Trieste even in seemingly wind-dominated situations.

5 Conclusions

In the paper we present a modeling analysis of the 24-hour marine drift by the windsurfer whose mast broke on 29 Oct 2018 16 UTC, during a 29 Oct 2018 Scirocco storm in the Northern Adriatic. We conduct an interview with the survivor in order to reconstruct his trajectory and its uncertainty. ~~We present numerical~~ The survivor knows the coast of the Gulf of Trieste very well, but had no GPS or watch on him during the drift. His reconstruction of the drift trajectory is therefore burdened with error. To estimate this error we used HF radar surface current measurements, which cover the second half of his drift, and employed them for upwind and upstream temporal back-propagation simulations starting at the beaching site at beaching time, both of which are exactly known. These back-propagation simulations were found to be largely consistent with

survivor's reconstruction, offering some confidence that while not perfect, the reconstructed trajectory can nevertheless serve as a qualitative guide for Lagrangian tracking.

We then present ocean circulation (NEMO), ~~wave (ECWAM),~~ atmosphere (ALADIN SI) and OpenDrift Lagrangian tracking models, used ~~in an attempt to hindcast this trajectory~~ to perform forward-propagation simulations of this trajectory, starting from the accident location. We present available ~~measurements from the~~ marine measurements (regional coastal buoy Vida and HF surface current radar) to qualitatively assess marine conditions in the Gulf of Trieste during the period of the drift.

~~Two Lagrangian tracking models were employed to compute the survivor's trajectory. First was OpenDrift , an established open source Lagrangian model, ingesting ocean currents and winds, and using past observational data to compute the drift of objects in marine environment. Neither Stokes drift nor wave data are~~ OpenDrift Lagrangian tracking model was employed using two types of marine drift parametrizations: "person in water" and "person with surf board". Stokes drift from a wave model was not explicitly included in OpenDrift ~~input~~ forcing data since these effects are already implicitly present in the downwind/crosswind drift parametrizations, deduced from observations.

~~The second Lagrangian tool was FlowTrack, a general purpose individual-based particle tracking model, written for Lagrangian tracking, water age and oil spill modelling in a marine environment. FlowTrack in principle allows for ingestion of wave data and Stokes drift computation prior to particle advection, but this option was not used for the simulations performed in this paper. The reason for this is that wave-induced drift has been shown to be of importance only for objects whose typical dimension is comparable to the wavelength of surface gravity waves scattering off the object. During the storm in question, surface gravity waves wavelengths surpassed 50 m, a value ten to twenty times longer than the length of the board or a person .~~

~~OpenDrift simulation were performed using two object types (PIW-1 and PERSON-POWERED-VESSEL-2), both indicating a rapidly growing search area which however extended along the reconstructed trajectory of the survivor's drift. The trajectories in both cases are spatially and temporally consistent with the reconstruction, but PERSON-POWERED-VESSEL-2 was more consistent with the survivor's trajectory estimate and yielded smaller and more precise SAR areas. Based on OpenDrift results, 6~~ To quantify performance of both drifter types, we calculated distributions of particle distances from the beaching location for both drifter types. Simulations using object type "person with surf board" yield best performance, with highest number of particles stranded within 5 km of the beaching location. Distribution maximum of "person with surf board" drifters is positioned about 15 km closer to the beaching point than the distribution maximum of "person in water" drifters. Both scenarios however lag behind the estimated drift which most likely results from NEMO model underestimation of surface currents during the event. For both drifter types accumulation of particles, stranded within 5 km of the beaching location, saturates roughly six hours after the ~~incident the search area spans 70 (45) km^2, rising more or less linearly to 650 (380) km^2 after 24 hours for PIW-1 (PERSON-POWERED-VESSEL-2) object type. This merely confirms that search and rescue response should be as rapid as possible~~ actual beaching time.

~~FlowTrack simulation currently lacks the capability of estimating the search and rescue area due to lack of downwind diffusion. Particle trajectories from FlowTrack are nevertheless defining an envelope within which the reconstructed trajectory takes place. The timing of the eventual beaching is also valid to within 3 hours~~ A control run of wind-only forcing was also

simulated and this setup was the worst performer of all three, indicating the importance of topographically constrained ocean currents in semi-enclosed basins like the Gulf of Trieste even in wind-dominated situations. ~~Nevertheless we find the OpenDrift approach better grounded for decision support during future search and rescue operations. Its downwind/crosswind parametrizations are based in observations and yield object class dependent search and rescue area. FlowTrack currently lacks any object class parametrization and simulations performed in this paper required constraining modeling parameters using existing literature. This is typically not temporally feasible during actual search and rescue missions~~Results in these paper indicate that any rescue response in the 29 Oct 2018 case would certainly benefit from OpenDrift simulations using "person with surf board" object type. However, while one can clearly benefit from using the most appropriate drift parametrization, lack of information during an actual event often complicates the decision on which parametrization to use.

It is also worth mentioning that given the location of the accident, a drift under Bora ~~conditions seems radically~~ wind conditions seems substantially more dangerous. ~~The~~ Bora is typically much colder and can, regardless of its short fetch, generate comparable marine conditions in Northern Adriatic, but its nautical direction is 60°, ~~i.e.~~ *i.e.* completely offshore in Northern Istria. Marine drift initiated in Umag (or, more likely, the Cape of Savudrija) during the Bora would have lasted days, and possibly more than a week ~~, if the object~~ if the person would get advected westward far enough to join Western Adriatic Current flowing southward along the Italian coast. Reliable and operational circulation models, coupled to Lagrangian tools like OpenDrift, would be an invaluable decision support for any rapid rescue attempt.

Author contributions. A.F. and M.L. set up NEMO for the Adriatic basin. A.F. performed NEMO simulations. M.L., S.E. and A.F. performed the OpenDrift simulations. S.E., C.R.S., D. D. and M. L. analyzed the HF radar data. M.L. devised the work plan and wrote the paper. All authors contributed to the final editing of the paper.

References

Allen, A. A. and Plourde, J. V.: Review of Leeway: Field Experiments and Implementation, Tech. rep., U. S. Coast Guard, 1999.

Breivik, Ø. and Allen, A. A.: An operational search and rescue model for the Norwegian Sea and the North Sea, Journal of Marine Systems, 69, 99 – 113, https://doi.org/https://doi.org/10.1016/j.jmarsys.2007.02.010, http://www.sciencedirect.com/science/article/pii/S0924796307000383, maritime Rapid Environmental Assessment, 2008.

Cavaleri, L., Bajo, M., Barbariol, F., Bastianini, M., Benetazzo, A., Bertotti, L., Chiggiato, J., Davolio, S., Ferrarin, C., Magnusson, L., Papa, A., Pezzutto, P., Pomaro, A., and Umgiesser, G.: The October 29, 2018 storm in Northern Italy – an exceptional event and its modeling, Progress in Oceanography, p. 102178, https://doi.org/https://doi.org/10.1016/j.pocean.2019.102178, https://www.sciencedirect.com/science/article/pii/S0079661119301089, 2019.

Craig, P. D. and Banner, M. L.: Modeling Wave-Enhanced Turbulence in the Ocean Surface Layer, Journal of Physical Oceanography, 24, 2546–2559, https://doi.org/10.1175/1520-0485(1994)024<2546:MWETIT>2.0.CO;2, https://doi.org/10.1175/1520-0485(1994)024<2546:MWETIT>2.0.CO;2, 1994.

Dagestad, K.-F., Röhrs, J., Breivik, Ø., and Ådlandsvik, B.: OpenDrift v1.0: a generic framework for trajectory modelling, Geoscientific Model Development, 11, 1405–1420, https://doi.org/10.5194/gmd-11-1405-2018, https://www.geosci-model-dev.net/11/1405/2018/, 2018.

Donlon, C. J., Martin, M., Stark, J. D., Roberts-Jones, J., Fiedler, E., and Wimmer, W.: The Operational Sea Surface Temperature and Sea Ice analysis (OSTIA), Remote Sensing of the Environment, 2012.

Dugstad, J. S., Koszalka, I. M., Isachsen, P. E., Dagestad, K.-F., and Fer, I.: Vertical Structure and Seasonal Variability of the Inflow to the Lofoten Basin Inferred From High-Resolution Lagrangian Simulations, Journal of Geophysical Research: Oceans, 124, 9384–9403, https://doi.org/10.1029/2019JC015474, https://agupubs.onlinelibrary.wiley.com/doi/abs/10.1029/2019JC015474, 2019.

Egbert, G. D. and Erofeeva, S. Y.: Efficient Inverse Modeling of Barotropic Ocean Tides, Journal of Atmospheric and Oceanic Technology, 19, 183–204, https://doi.org/10.1175/1520-0426(2002)019<0183:EIMOBO>2.0.CO;2, https://doi.org/10.1175/1520-0426(2002)019<0183:EIMOBO>2.0.CO;2, 2002.

Engedahl, H.: Use of the flow relaxation scheme in a three-dimensional baroclinic ocean model with realistic topography, Tellus A, 47, 365–382, https://doi.org/10.1034/j.1600-0870.1995.t01-2-00006.x, https://onlinelibrary.wiley.com/doi/abs/10.1034/j.1600-0870.1995.t01-2-00006.x, 1995.

Fischer, C., Montmerle, T., Berre, L., Auger, L., and Ştefănescu, S. E.: A lateral boundary formulation for multi-level prediction models, Quarterly Journal of Royal Meteorological Society, 102, 1976.

Fischer, C., Montmerle, T., Berre, L., Auger, L., and Ştefănescu, S. E.: An overview of the variational assimilation in the ALADIN/France numerical weather-prediction system, Quarterly Journal of Royal Meteorological Society, 131, 2005.

Gerard, L., Piriou, J.-M., Brožková, R., Geleyn, J.-F., and Banciu, D.: Cloud and precipitation parameterization in a meso-gamma-scale operational weather prediction model, Monthly Weather Review, 137, 2009.

Gurgel, K.-W., Antonischki, G., Essen, H.-H., and Schlick, T.: Wellen Radar (WERA): a new ground-wave HF radar for ocean remote sensing, Coastal Engineering, 37, 219 – 234, https://doi.org/https://doi.org/10.1016/S0378-3839(99)00027-7, 1999.

Hackett, B., Breivik, Ø., and Wettre, C.: Forecasting the Drift of Objects and Substances in the Ocean, pp. 507–523, Springer Netherlands, Dordrecht, https://doi.org/10.1007/1-4020-4028-8_23, https://doi.org/10.1007/1-4020-4028-8_23, 2006.

567 Large, W. G. and Yeager, S. G.: Diurnal to Decadal Global Forcing for Ocean and Sea-Ice Models: The Data Sets and Flux Climatologies,
568   https://nomads.gfdl.noaa.gov/nomads/forms/mom4/CORE.html, 2004.

569 Ličer, M., Smerkol, P., Fettich, A., Ravdas, M., Papapostolou, A., Mantziafou, A., Strajnar, B., Cedilnik, J., Jeromel, M., Jerman, J., Petan,
570   S., Malačič, V., and Sofianos, S.: Modeling the ocean and atmosphere during an extreme bora event in northern Adriatic using one-way
571   and two-way atmosphere-ocean coupling, Ocean Science, 12, 71–86, https://doi.org/10.5194/os-12-71-2016, https://www.ocean-sci.net/
572   12/71/2016/, 2016.

573 Madec, G.: NEMO ocean engine, Tech. rep., Institut Pierre-Simon Laplace (IPSL), https://www.nemo-ocean.eu/wp-content/uploads/
574   NEMO_book.pdf, 2008.

575 Malačič, V.: Wind Direction Measurements on Moored Coastal Buoys, Journal of Atmospheric and Oceanic Technology, 36, 1401–1418,
576   https://doi.org/10.1175/JTECH-D-18-0171.1, https://doi.org/10.1175/JTECH-D-18-0171.1, 2019.

577 Malačič, V., Petelin, B., and Vodopivec, M.: Topographic control of wind-driven circulation in the northern Adriatic, Journal of Geophysical
578   Research: Oceans, 117, https://doi.org/10.1029/2012JC008063, https://agupubs.onlinelibrary.wiley.com/doi/abs/10.1029/2012JC008063,
579   2012.

580 Röhrs, J., Dagestad, K.-F., Asbjørnsen, H., Nordam, T., Skancke, J., Jones, C. E., and Brekke, C.: The effect of vertical mixing on the
581   horizontal drift of oil spills, Ocean Science, 14, 1581–1601, https://doi.org/10.5194/os-14-1581-2018, https://www.ocean-sci.net/14/1581/
582   2018/, 2018.

583 Strajnar, B., Žagar, N., and Berre, L.: Impact of new aircraft observations Mode-S MRAR in a mesoscale NWP model, Journal of Geophysical
584   Research: Atmospheres, 2015.

585 Strajnar, B., Cedilnik, J., Fettich, A., Ličer, M., Pristov, N., Smerkol, P., and Jerman, J.: Impact of two-way coupling and sea-surface tem-
586   perature on precipitation forecasts in regional atmosphere and ocean models, Quarterly Journal of the Royal Meteorological Society, 145,
587   228–242, https://doi.org/10.1002/qj.3425, https://rmets.onlinelibrary.wiley.com/doi/abs/10.1002/qj.3425, 2019.